Resource

Cell Chemical Biology

Beyond DPPH: Use of Fluorescence-Enabled Inhibited Autoxidation to Predict Oxidative Cell Death Rescue

Graphical Abstract

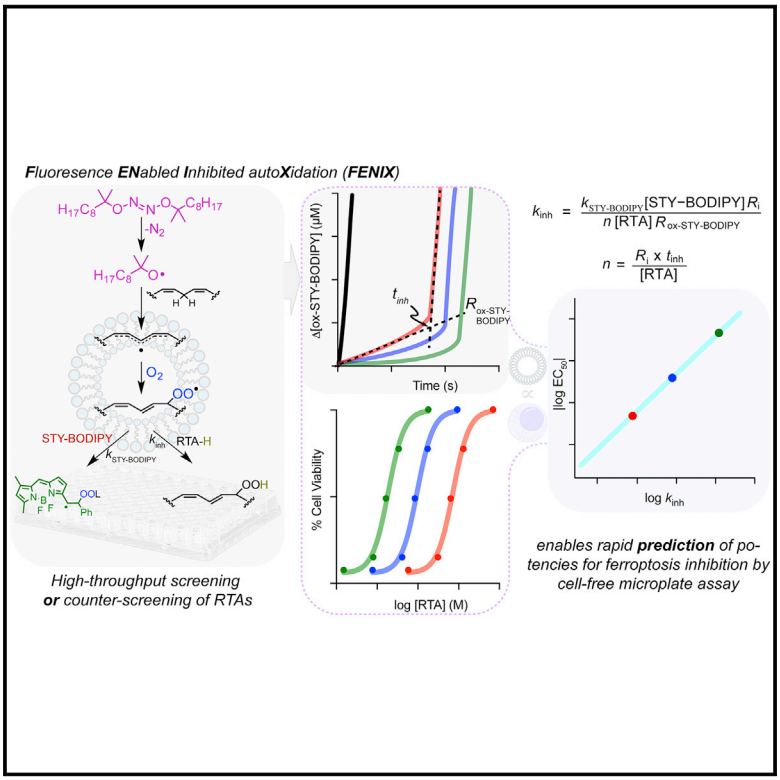

Authors

Ron Shah, Luke A. Farmer, Omkar Zilka, Antonius T.M. Van Kessel, Derek A. Pratt

Correspondence

dpratt@uottawa.ca

In Brief

Shah et al. develop a fluorescence-enabled inhibited autoxidation (FENIX) approach that permits accurate quantitation of radical-trapping antioxidant activity in phospholipid bilayers. The methodology is far superior to existing assays (e.g., DPPH) and enables reliable prediction of the anti-ferroptotic potency of redox-active compounds. The approach is easily amenable to high-throughput screening.

Highlights

- FENIX enables screening or counter-screening of lipid peroxidation inhibitors
- Equally simple to the DPPH assay, but relays information on kinetics and stoichiometry
- FENIX in liposomes predicts the anti-ferroptotic potency of antioxidants in cells
- H-bonding to the phospholipid head group attenuates RTA activity in lipid bilayers

Shah et al., 2019, Cell Chemical Biology *26*, 1–14
November 21, 2019
https://doi.org/10.1016/j.chembiol.2019.09.007

CellPress

Please cite this article in press as: Shah et al., Beyond DPPH: Use of Fluorescence-Enabled Inhibited Autoxidation to Predict Oxidative Cell Death Rescue, Cell Chemical Biology (2019), https://doi.org/10.1016/j.chembiol.2019.09.007

Cell Chemical Biology
Resource

Beyond DPPH: Use of Fluorescence-Enabled Inhibited Autoxidation to Predict Oxidative Cell Death Rescue

Ron Shah,[1] Luke A. Farmer,[1] Omkar Zilka,[1] Antonius T.M. Van Kessel,[1] and Derek A. Pratt[1,2,*]
[1]Department of Chemistry and Biomolecular Sciences, University of Ottawa, Ottawa, ON K1N 6N5, Canada
[2]Lead Contact
*Correspondence: dpratt@uottawa.ca
https://doi.org/10.1016/j.chembiol.2019.09.007

SUMMARY

"Antioxidant activity" is an often invoked, but generally poorly characterized, molecular property. Several assays are available to determine antioxidant activity, the most popular of which is based upon the ability of a putative antioxidant to reduce 2,2-diphenyl-1-picrylhydrazyl. Here, we show that the results of this assay do not correlate with the potency of putative antioxidants as inhibitors of ferroptosis, the oxidative cell death modality associated with (phospho)lipid peroxidation. We subsequently describe our efforts to develop an approach that quantifies the reactivity of putative antioxidants with the (phospho)lipid peroxyl radicals that propagate (phospho)lipid peroxidation (dubbed FENIX [fluorescence-enabled inhibited autoxidation]). The results obtained with FENIX afford an excellent correlation with anti-ferroptotic potency, which facilitates mechanistic characterization of ferroptosis inhibitors, and reveals the importance of H-bonding interactions between antioxidant and phospholipid that underlie both the lackluster antioxidant activity of phenols under physiologically relevant conditions and the emergence of arylamines as inhibitors of choice.

INTRODUCTION

Lipid peroxidation, the radical-mediated chain reaction that converts lipids into lipid hydroperoxides (and a myriad of other oxidation products) has been implicated in the pathogenesis of virtually every type of degenerative disease (Barnham et al., 2004; Finkel and Holbrook, 2000; McIntyre and Hazen, 2010; Di Paolo and Kim, 2011). The current molecular level understanding of lipid peroxidation (simplified mechanism, Figure 1A) (Yin et al., 2011; Zielinski and Pratt, 2017) has been established largely on the basis of detailed chemical studies of hydrocarbon autoxidation, the process primarily responsible for the oxidative degradation of petroleum-derived products (Denison and Harle, 1949; Frank, 1950). Therefore, it has long been thought that radical-trapping antioxidants (RTAs) (Ingold, 1961; Ingold and Pratt, 2014), which are preservatives added to essentially every type of hydrocarbon-based commercial and/or industrial product, may slow the onset and development of degenerative disease. Despite considerable investigation, the use of RTAs in commercial and/or industrial applications has not translated to results in the clinic. Put simply, there has been overwhelming evidence against antioxidant intervention as a useful strategy for degenerative disease treatment and/or prevention in humans (Lonn, 2005; Semba et al., 2014; Sesso et al., 2012).

At the root of many clinical trials of antioxidant treatment and/or supplementation is the characterization of potential antioxidants using assays of antioxidant activity. The most common assays involve the decolorization of a highly absorbing oxidant by reduction with a putative antioxidant. Examples include 2,2-diphenyl-1-picrylhydrazyl (DPPH) (Blois, 1958), the ferric reducing ability of plasma (Benzie and Strain, 1996), oxygen radical absorbance capacity (ORAC) (Cao et al., 1993), and 2,2′-azino-bis(3-ethylbenzothiazoline-6-sulfonic acid (ABTS) (Re et al., 1999). The limitations of these assays have been elaborated upon elsewhere. Most importantly, they fail to provide information about the reactivity of a potential inhibitor toward the kinetically relevant oxidizing species—a propagating lipid peroxyl radical (i.e., k_{inh}; Figure 1A) (Ingold, 1961; Ingold and Pratt, 2014). This is where the divergence between industrial compound development and potential preventive/therapeutic compounds originates. Industrial antioxidants, such as hindered phenols and aromatic amines, are developed and tested in a context that is highly similar to their eventual application—and where the experimental methods measure relevant properties, such as oxidation product formation or viscosity changes (Gray, 1978; Naidu et al., 1984; Shah and Pratt, 2016). This underscores the need for methods that assay RTA activity under physiologically relevant conditions. Of course, it must be acknowledged that modeling a lubricant or polymer is far easier than a cell, tissue, or whole organism.

The recent characterization of ferroptosis (Dixon et al., 2012; Friedmann Angeli et al., 2014; Stockwell et al., 2017), a form of regulated necrosis associated with the accumulation of (phospho)lipid oxidation products, and the development of new cell-based tools to study it, have provided an unprecedented capability to investigate the link between lipid peroxidation and disease. Ferroptosis can be induced in a variety of ways, but the quintessential—and arguably most direct—method is to interfere with the cell's ability to detoxify (phospho)lipid hydroperoxides. Left to accumulate, the hydroperoxides can undergo one-electron reduction by ferrous iron, or other one-electron reductants, to produce lipid-derived alkoxyl radicals that can initiate further lipid peroxidation chain reactions. Glutathione peroxidase 4 (GPX4), a selenoprotein that catalyzes the glutathione-mediated reduction of hydroperoxides to alcohols, is

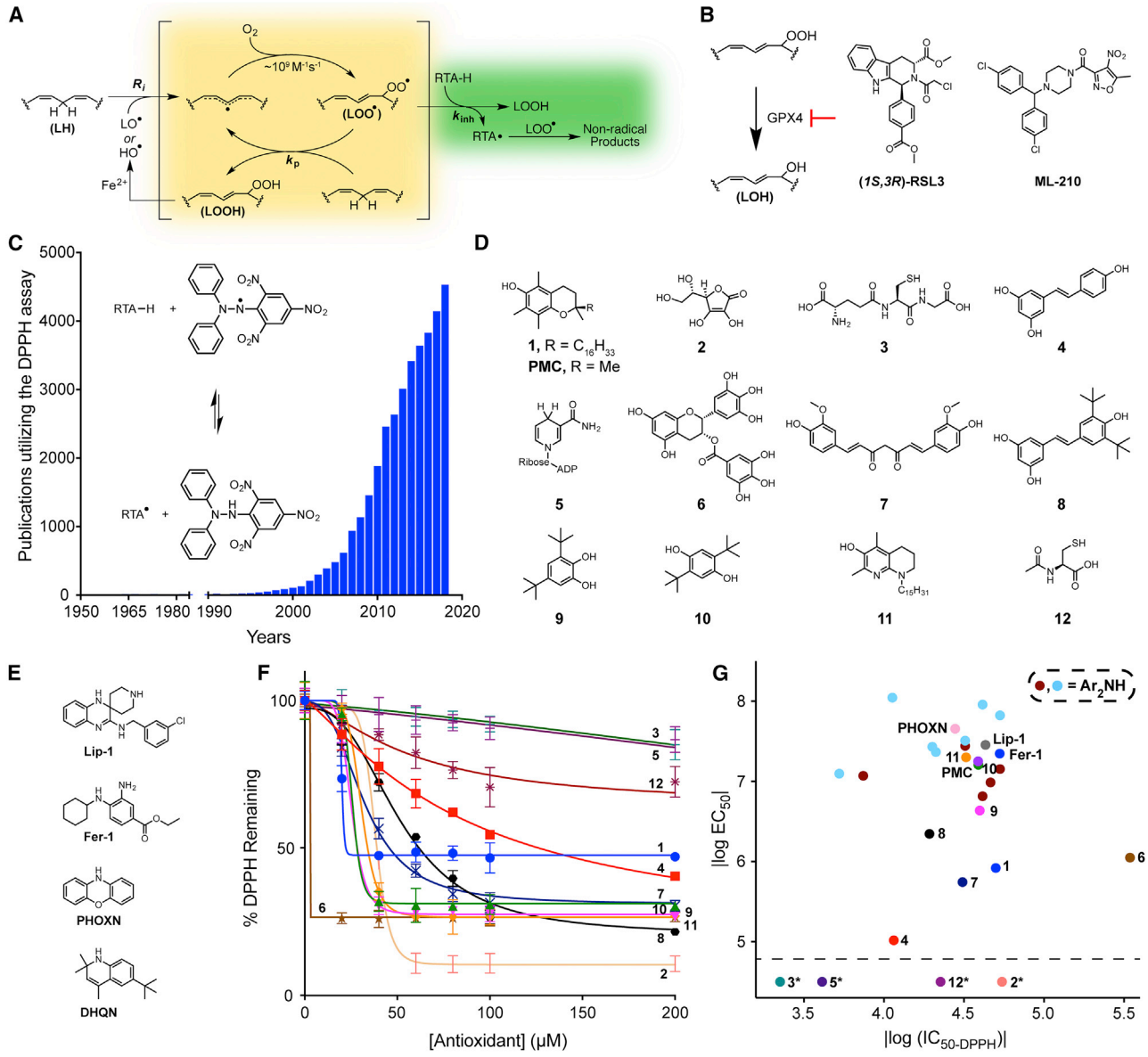

Figure 1. Lipid Peroxidation, its Inhibition by RTAs, and the Inadequacy of the DPPH Assay to Account for the Anti-ferroptotic Activity of RTAs

(A) Simplified mechanism of lipid peroxidation (autoxidation) and its inhibition by RTAs.

(B) Inhibition of GPX4 leads to the induction of ferroptosis.

(C) The DPPH assay (inset) and trends in publications with the keyword "DPPH" in either the article title or abstract. Data obtained by searching the keyword DPPH on Scopus. The results were exported into Excel and plotted using GraphPad Prism.

(D) Structures of purported natural product "antioxidants" and some related derivatives used in this study.

(E) Structures of potent ferroptosis inhibitors.

(F) The titration of DPPH (100 μM) with compounds **1**–**12**. Error bars represent the standard deviation obtained from at least three independent measurements.

(G) Plot of IC_{50} for DPPH quenching versus EC_{50} for inhibition of RSL3-induced ferroptosis in Pfa1 mouse embryonic fibroblasts (MEFs). Data in light blue and brown correspond to the diarylamines (Ar_2NH) in Figure S1A (R^2 = 0.01). Data points labeled with an asterisk did not inhibit ferroptosis up to 10 μM.

Data are presented as mean ± SD. See also Figure S1.

the unique enzyme that can operate directly on phospholipid hydroperoxides—and is therefore generally considered the master regulator of ferroptosis (Conrad and Friedmann Angeli, 2015; Friedmann Angeli et al., 2014; Seibt et al., 2019).

The inhibition of GPX4 (e.g., with RSL3 [Dixon et al., 2012; Yang and Stockwell, 2008] or ML210 [Viswanathan et al., 2017; Weiwer et al., 2012]) (Figure 1B), deletion of the gene encoding it (Friedmann Angeli et al., 2014; Seiler et al., 2008), or suppression of its expression, present the ideal basis for cell-based assays of inhibitors of lipid peroxidation. Indeed, such assays have been used to screen compound libraries to identify some of the most potent ferroptosis inhibitors to date (e.g.,

ferrostatin-1 [Dixon et al., 2012; Skouta et al., 2014] and liproxstatin-1 [Friedmann Angeli et al., 2014]) (Figure 1E). However, because cellular lipid peroxidation can be modulated in other ways (e.g., the incorporation of [non]-oxidizable polyunsaturated fatty acids in the lipid bilayer) (Doll et al., 2017; Magtanong et al., 2019), these cell-based assays need to be complemented by a method that can unambiguously resolve intervention in the propagation of lipid peroxidation. Such a method would enable resolution of inhibitors that do not act as antioxidants, providing insight on other mechanisms that may contribute to ferroptosis and/or its regulation. Building upon previous work wherein we showed that a small amount of an autoxidizable chromophore (i.e., STY-BODIPY or PBD-BODIPY) can be used to monitor hydrocarbon autoxidations and their inhibition by RTAs (Haidasz et al., 2016), we now report a microplate-based assay that enables screening for, and assessment of, RTA activity in phospholipid bilayers. We relay its development in an effort to highlight the important aspects that must be considered to accurately determine antioxidant efficacy in a cellular context. These aspects clarify why phenolic antioxidants are not particularly effective under physiologically relevant conditions, why aromatic amines are strongly preferred, and serve to guide future design and/or optimization of ferroptosis inhibitors.

RESULTS

The DPPH Assay Fails to Predict Cytoprotective Potency of Putative Antioxidants

Among the aforementioned measures of antioxidant activity, the DPPH assay (Figure 1C) is arguably the most popular method. Introduced in 1922 (Goldschmidt and Renn, 1922), DPPH was mainly used in electron paramagnetic resonance spectroscopy as a calibrant and standard. It was not until 1958 that it was used to determine antioxidant activity (Blois, 1958). Ever since, the use of DPPH to determine antioxidant activity has seen a dramatic increase that roughly coincides with the recognition of "oxidative stress" as being relevant in human health. Despite the well-documented shortcomings of the DPPH assay (Li and Pratt, 2015; Amorati and Valgimigli, 2015; Foti, 2015; Niki, 2010), its popularity for the assessment of antioxidant activity prompted us to assess its use for the prediction of ferroptosis inhibitor potency. In fact, others have used the results of DPPH assays to provide insight on the mechanism of inhibition of ferroptosis by small molecules (Dixon et al., 2012; Doll et al., 2017; Gao et al., 2015; Liu et al., 2015; Magtanong et al., 2019). Our test set included ferrostatin-1 (Fer-1) and liproxstatin-1 (Lip-1), the two quintessential ferroptosis inhibitors, a variety of diarylamines (Figures 1E and S1A) that we recently demonstrated to be equivalent to—or better than—Fer-1 and Lip-1 (Shah et al., 2017), some representative phenolic antioxidants including Nature's premier RTA, α-tocopherol (Burton and Ingold, 1986), and the related, but much more potent tetrahydronaphthyridinol derivative (Li et al., 2013; Zilka et al., 2017). We also included a variety of purported antioxidants of varying hydrophilicity/hydrophobicity, including ascorbic acid, glutathione, N-acetylcysteine, NADPH, a hydroquinone, a catechol, curcumin, resveratrol, and epigallocatechin gallate, the so-called "green tea polyphenol" (Figure 1D).

The DPPH assay was carried out in a 96-well microplate wherein various concentrations of compounds were incubated with 100 μM DPPH in ethanol for 30 min before determination of the absorbance at 517 nm using a microplate reader (Cos et al., 2003). The half maximal inhibitory concentration (IC_{50}) values were calculated by fitting the percentage of the DPPH radical remaining after the incubation period, as is customary (Figures 1F, S1B, and S1C) (Blois, 1958; Chen et al., 2013; Kedare and Singh, 2011). The most potent RTA in this assay was the polyphenolic natural product epigallocatechin gallate (**6**), with an IC_{50} of 2.9 μM, while glutathione (**3**) was the least potent with an IC_{50} of 445 μM. These results are consistent with literature precedent, wherein it is reported that the efficacy for DPPH quenching increased in the following order: glutathione (**3**) > hydroquinone (**10**) > catechol (**9**) > ascorbic acid (**2**) $\approx$ epigallocatechin gallate (**6**) (Xie and Schaich, 2014). Surprisingly, we found that the IC_{50} values for glutathione (**3**) and N-acetylcysteine (**12**) were 10-fold different, despite the fact that both molecules have the same redox-active thiol moiety. It is reported that natural product resveratrol (**4**) and its corresponding *tert*-butylated analog (**8**) have different RTA activities, yet they had very similar IC_{50} values (Matsuura et al., 2015), suggesting that the assay is not sensitive enough to discern alkyl substituent effects. It was also difficult to observe any trends in results with arylamines—the IC_{50} values were in a very narrow range (18–35 μM) despite the fact that they are reported to have vastly different RTA activities (Shah et al., 2017).

The potencies of these compounds as ferroptosis inhibitors were then determined in mouse embryonic fibroblasts (Friedmann Angeli et al., 2014) treated with the GPX4 inhibitor RSL3 (Yang and Stockwell, 2008) (Figure S1D). The half maximal effective concentration (EC_{50}) values are plotted alongside the IC_{50} values obtained from the DPPH assay in Figure 1G, wherein no correlation is evident. Most naturally occurring phenolic antioxidants (**1**, **4**, **6**, and **7**) were modest inhibitors of cell death with EC_{50} > 1 μM, whereas the synthetic derivatives (**8**–**11**) were more potent with EC_{50} values <450 nM. As expected from previous work, aromatic amines, including Fer-1, Lip-1, and phenoxazine (PHOXN) were the most potent compounds. On the other hand, water-soluble compounds (**2**, **3**, **5**, and **12**) failed to rescue cells from ferroptosis (up to 10 μM), presumably due to their inability to traverse the lipid bilayer (ClogP < –0.5). Of course, this is not captured in the DPPH assay. Overall, it is clear that, despite its popularity, the DPPH assay is a poor predictor of ferroptosis inhibition as demonstrated by the clear lack of a correlation in Figure 1G (R^2 = 0.01).

Initial Efforts to Develop a Predictive Assay

The rate-limiting step in the propagation of the lipid peroxidation chain reaction involves the abstraction of an H-atom from the lipid by a peroxyl radical (Yin et al., 2011; Zielinski and Pratt, 2017) (Figure 1A). (It should be mentioned that some lipids, e.g. cholesterol, can also propagate by addition of a peroxyl radical to an unsaturation Zielinski and Pratt, 2019). An effective RTA must compete with phospholipids for this peroxyl radical and yield an RTA-derived radical that is persistent (i.e., does not propagate the chain reaction) (Ingold, 1961; Ingold and Pratt, 2014). Thus, an assay that is based upon this *kinetic competition* is expected to be better able to predict the potency of putative RTAs in cells. A short time ago, we developed the basis for

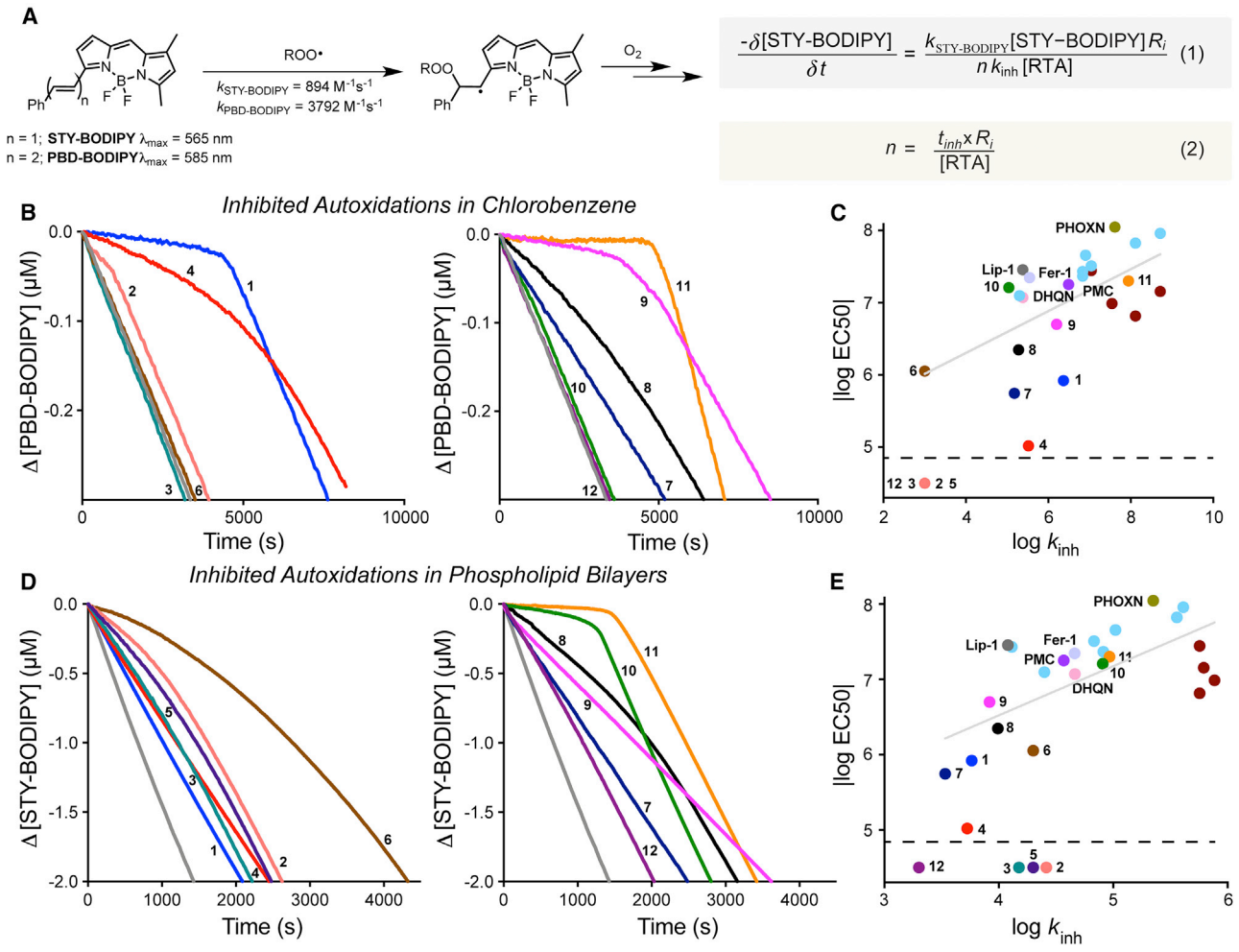

Figure 2. The Co-autoxidation of either STY-BODIPY or PBD-BODIPY and an Appropriate Substrate Enables the Rapid Determination of RTA Kinetics and Stoichiometry under a Variety of Conditions

(A) The reaction of STY-BODIPY and PBD-BODIPY with peroxyl radicals can be used as a signal carrier in inhibited co-autoxidations to obtain inhibition rate constants (k_{inh}) and stoichiometries (n) of added RTAs. [BODIPY] = dye concentration at t = 0 (M); n = stoichiometry; [RTA] = antioxidant concentration (M); R_i = rate of initiation; k_{BODIPY} = rate constant of propagation; t_{inh} = inhibition time (s).

(B) Representative co-autoxidations of PBD-BODIPY (10 μM) and 1-hexadecene (2.8 M) initiated by azobisisobutyronitrile (AIBN) (6 mM) in chlorobenzene at 37°C (gray) and inhibited by 2 μM of compounds **1**–**12**.

(C) Correlation of inhibition rate constants determined in chlorobenzene and EC_{50} values from RSL3-induced ferroptosis in Pfa1 MEFs (R^2 = 0.29).

(D) Representative co-autoxidations of STY-BODIPY (10 μM) embedded liposomes of egg phosphatidylcholine (1 mM) suspended in PBS (10 mM) at pH 7.4 initiated by MeOAMVN (0.2 mM) at 37°C (gray) and inhibited by 2 μM of compounds **1**–**12**.

(E) Correlation of inhibition rate constants determined in liposomes and EC_{50} values from RSL3-induced ferroptosis in Pfa1 MEFs (R^2 = 0.42). Compounds below the dashed line did not inhibit ferroptosis up to 10 μM.

Data show mean ± SD from three independent experiments. See also Figure S1.

such an assay. The experiment involves the competition of an RTA and a highly colored and highly oxidizable probe for the peroxyl radicals that propagate the autoxidation of a hydrocarbon substrate. Thus, by adding a small amount of this probe molecule (i.e., STY-BODIPY or PBD-BODIPY, Figure 2A) to an autoxidizable substrate, the progress of the reaction and its inhibition by RTAs can be readily monitored by conventional spectrophotometry (Haidasz et al., 2016). Moreover, since the rate constant for the reaction of the probe molecule and a peroxyl radical can be independently determined, the rate constant for the reaction of the RTA and a peroxyl radical (k_{inh}) can be derived from the initial rate of the inhibited autoxidation where this competition takes place (Equation 1 in Figure 2A, see Supplemental Information for derivation of k_{inh}).

In preliminary work, we used this method to determine the apparent inhibition rate constants (k_{inh}) for Lip-1, Fer-1, and a variety of diarylamines that were found to be potent inhibitors of ferroptosis (Shah et al., 2017; Zilka et al., 2017). We have since expanded the set of antioxidants investigated with this approach to those with which we obtained the above data for reactions with DPPH. Representative data from co-autoxidations of PBD-BODIPY and 1-hexadecene in chlorobenzene are included in Figure 2B

(rate constants are shown in Figure S1E). It is important to note that the autoxidations were initiated with azobisisobutyronitrile and that the rate of initiation (R_i), which is important in determining the stoichiometry of radical-trapping (or the number *n* of peroxyl radicals trapped per molecule of RTA, Equation 2 in Figure 2A, see Supplemental Information on derivation), was determined using the inhibition time of 2,2,5,7,8-pentamethyl-6-chromanol (PMC), the truncated analog of vitamin E, for which *n* = 2 (Burton and Ingold, 1986). The kinetic data roughly trend with the cytoprotective potencies of the test compounds, although the correlation is rather poor, with a significant amount of scatter still evident in Figure 2C (R^2 = 0.29). Therefore, although these experiments report on the kinetics of reactions of antioxidants with peroxyl radicals they still lack predictive capacity when it comes to the potency of antioxidants as ferroptosis inhibitors.

In the aforementioned preliminary work, a slightly better correlation between k_{inh} and cytoprotective potency was obtained when the kinetics were determined from 2,2′-azobis(4-methoxy-2,4-dimethylvaleronitrile) (MeOAMVN)-initiated co-autoxidations of STY-BODIPY and the polyunsaturated lipids of unilamellar liposomes of egg phosphatidylcholine—conditions expected to more closely mimic the cellular membrane and the membranes of subcellular compartments (Figure 2D). However, once again, an expansion of the initial dataset to include all of the compounds investigated above did not lead to a substantial improvement (Figure 2E) (R^2 = 0.42). Interestingly, while the data for many compounds seem to correlate better, most of the "outliers" segregate into two distinct groups: water-soluble compounds that were measured to be good RTAs in liposomes, but are ineffective in cells (i.e., **2**, **3**, and **5**), and water-soluble diarylamines that are among the most potent of RTAs, but are less potent in cells than expected (brown circles). These results suggest that the assay conditions developed to date are still not fully representative of the lipid peroxidation that drives ferroptotic cell death. Since we anticipated that efforts to optimize assay parameters using the current protocol could prove prohibitively time consuming, we first sought to develop a high-throughput version of our co-autoxidation approach to enable us to more rapidly survey reaction conditions.

Optimization of Co-autoxidation Conditions

Until now, reaction progress in STY-BODIPY (or PBD-BODIPY) co-autoxidations has been monitored by the decrease in absorbance of the chromophore at its λ_{max} as it reacts with peroxyl radicals (Figure 3A). However, we anticipated that a fluorescence-based method would be better suited for a more high-throughput microplate-based assay. The narrow Stokes shift in STY-BODIPY prompted to test several excitation wavelengths to determine which would afford optimal increase in green fluorescence. We settled on excitation at 488 nm and emission at 518 nm (Figure 3B).

Expectedly, the fluorescence of the probe increased linearly over time when it was added as a signal carrier during the autoxidation of 1 mM egg PC liposomes (extruded to 100 nm). To enable quantitation of the amount of STY-BODIPY (0.2–1 μM) that had been oxidized, we determined the plateau in fluorescence as a function of [STY-BODIPY]. The plateau represents the point at which the styryl side chain has undergone oxidation, but the slower reaction of peroxyl radicals with the BODIPY core has yet to take place (at which point the fluorescence decreases, see Figure S2A) (Krumova et al., 2012). Plotting the maximal fluorescence as a function of dye concentration resulted in a response factor of 7.5 × 10^4 relative fluorescence units (RFU)/μM (Figure S2B). This enabled the determination of the concentration of the oxidized probe as a function of time, which is necessary to derive k_{inh} from Equation 1 in Figure 2A. With a microplate-based method available to follow reaction progress in liposome autoxidations, we surveyed a variety of conditions to establish a model capable of predicting the potency of ferroptosis inhibitors in cells using the apparent inhibition rate constants in liposomes. To expand on our preliminary work, we tested both water-soluble (2,2-azobis(2-amidinopropane)dihydrochloride (AAPH), 1 mM) and lipid-soluble (MeOAMVN, 0.2 mM) initiators in 1 mM egg PC liposomes (Figures 3C and 3D, respectively). Initially, autoxidations inhibited using PMC (4 μM), PHOXN (4 μM), glutathione (GSH) (10 μM), ascorbic acid (10 μM), or NAC (50 μM) (Figure 3E, left and 3F, left) were carried out. Surprisingly, although the values of k_{inh} determined for the lipophilic RTAs (PMC and PHOXN) varied with initiator, those of the water-soluble RTAs (GSH, NAC and ascorbic acid) did not (cf. Table S1). Since AAPH is water-soluble, it is expected that the water-soluble RTAs inhibit STY-BODIPY oxidation by reacting directly with the initiator-derived radicals before initiating lipid peroxidation, whereas the lipophilic RTAs require import of the radicals from the aqueous phase to the lipid phase to react, and therefore compete with lipids for peroxyl radicals. MeOAMVN, on the other hand, is considered to be a lipid-soluble initiator, so it is expected that the efficacy with which water-soluble RTAs inhibit the autoxidation would be substantially worse than in the AAPH-initiated autoxidations. This was obviously not the case. Because small unilamellar vesicles have large curvature resulting in increased dynamics of the bilayer, we wondered whether this effect was simply due to the facile diffusion of water-soluble RTAs into the liposomal membrane. However, a similar experiment with 200 nm liposomes afforded equivalent results, wherein water-soluble RTAs were still highly potent in MeOAMVN-initiated autoxidations (Figure S2E).

These findings suggested that the water-soluble RTAs were reacting directly with MeOAMVN-derived radicals at the lipid-aqueous interface, such that these RTAs compete directly with initiation of lipid peroxidation. Expanding the test set of compounds investigated to the "full" set examined in Figures 1 and 2, reinforced the trends observed with the small test set and our preliminary efforts—particularly, that water-soluble compounds appear to be reacting directly with initiator-derived radicals (Figure 3G) (R^2 = 0.40) (Shah et al., 2017). Indeed, when we calculated the kinetic chain lengths for both reaction systems—even in the absence of RTA—they were found to be less than 1 (Table S2), suggesting that the oxidations were not radical chain reactions.

To ensure that the oxidations were being carried out under radical chain condition (i.e., rate of oxidation >> rate of initiation), such that they can be considered *bona fide* autoxidations, we increased the lipid concentration to 20 mM in egg PC while keeping the rate of initiation the same (Figures 3E, right, and 3F, right). Doing so gave kinetic chain lengths of 8 and 12 for the AAPH- and MeOAMVN-initiated oxidations, respectively. Under these conditions, the water-soluble RTAs were far less effective than under non-chain conditions, consistent with the phase-separation of the lipid peroxyl radicals from the water-soluble antioxidants. Encouraged by these results, we carried out inhibited autoxidations with the full test set of compounds under these

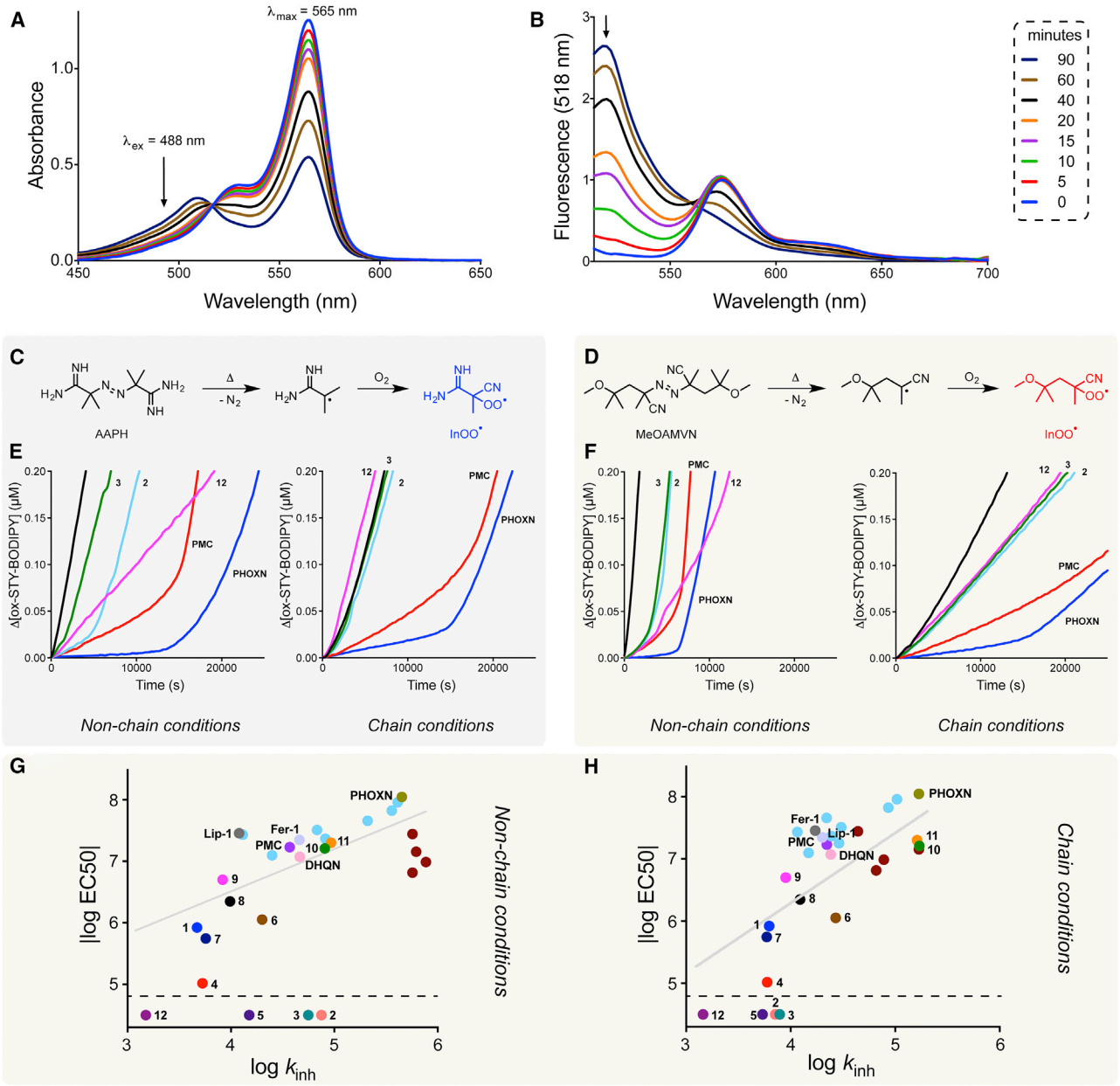

Figure 3. RTA Kinetics Derived from STY-BODIPY/Phospholipid Co-autoxidations Initiated with Conventional Radical Initators do not Correlate well with Anti-ferroptotic Potency

(A and B) Co-autoxidation of STY-BODIPY (1 μM)-embedded liposomes of egg PC (1 mM) suspended in PBS (10 mM) at pH 7.4 initiated with MeOAMVN (0.2 mM) monitored by either absorbance (A) or fluorescence (B).

(C–F) AAPH (C) and MeOAMVN (D) radical initiators. Representative co-autoxidations of STY-BODIPY (1 μM)-embedded liposomes of egg PC (1 or 20 mM) initiated by either (E) AAPH (1 mM, black) or (F) MeOAMVN (0.2 mM, black) and inhibited by PMC (4 μM, red), phenoxazine (4 μM, blue), ascorbic acid (10 μM, cyan), glutathione (10 μM, green), or NAC (50 μM, magenta).

(G and H) Correlation of inhibition rate constants determined in either 1 mM (R^2 = 0.40) (G) or 20 mM (R^2 = 0.58) (H) liposomes and EC_{50} values from RSL3-induced ferroptosis in Pfa1 MEFs. Compounds below the dashed line did not inhibit ferroptosis up to 10 μM.

Data show mean ± SD of n = 3 wells from a 96-well plate from one representative of three independent experiments. See also Figure S2 and Table S1.

conditions (Figure 3H). Surprisingly, the resultant correlation of EC_{50} with k_{inh} improved only marginally (R^2 = 0.58) relative to that obtained when using data from the oxidations carried out under non-chain conditions (Figure 3G), suggesting that interception of initiator-derived radicals by water-soluble or amphiphilic RTAs may still be a problem. Indeed, we found that no consumption of STY-BODIPY took place in MeOAMVN-treated liposomes, which were subsequently purified by size-exclusion chromatography (SEC) (see Figure 4B), indicating that MeOAMVN is poorly incorporated into lipid bilayers and must

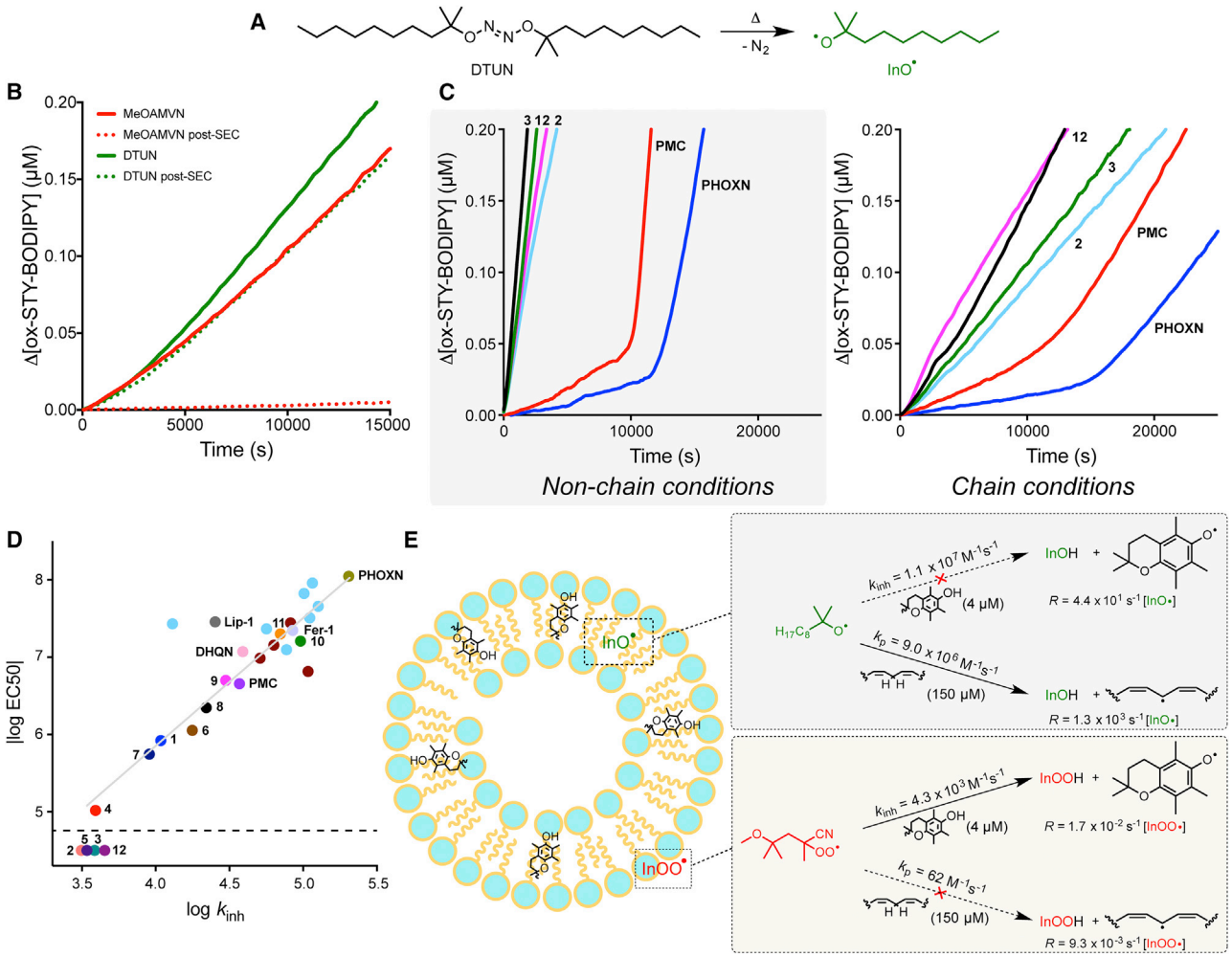

Figure 4. Optimized FENIX Assay Conditions Yields Kinetic Data that Predicts the Potency of RTAs to Subvert Ferroptosis

(A) The DTUN radical initiator.

(B) Purification of liposomes by size-exclusion chromatography following initiator additions removed MeOAMVN, but not DTUN, indicating that MeOAMVN is not efficiently incorporated into the liposome.

(C) Representative co-autoxidations of STY-BODIPY (1 μM)-embedded liposomes of egg PC (1 or 20 mM) initiated by DTUN (0.2 mM, black) and inhibited by either PMC (4 μM, red), phenoxazine (4 μM, blue), ascorbic acid (10 μM, cyan), glutathione (10 μM, green), or NAC (50 μM, magenta).

(D) Correlation of inhibition rate constants determined in liposomes and EC_{50} values from RSL3-induced ferroptosis in Pfa1 MEFs ($R^2 = 0.84$). Compounds below the dashed line did not inhibit ferroptosis up to 10 μM.

(E) Model of liposome and associated kinetics accounting for the difference in reactivity of MeOAMVN- and DTUN-derived initiating radicals. Data show mean ± SD of n = 3 wells from a 96-well plate from one representative of three independent experiments.

See also Figure S3 and Table S1.

reside primarily in the interfacial region. Coextrusion of MeOAMVN with egg PC liposomes followed by SEC resulted in similar rates of STY-BODIPY consumption to liposomes to which MeOAMVN was added directly (without SEC), suggesting that MeOAMVN can be efficiently incorporated in this manner. However, initiator addition after extrusion is preferable to prevent autoxidation during liposome formation, handling, and storage (of refrigerated stock liposome suspensions).

Use of a Lipophilic Hyponitrite Initiator Completes a Predictive Assay

Hyponitrites, such as di-*tert*-butyl hyponitrite (DTBN), were often used to initiate lipid autoxidation (Barclay et al., 1986; Kigoshi et al., 1993) before the widespread adoption of MeOAMVN (Noguchi et al., 1998). The commercial availability of MeOAMVN, its well-characterized kinetics of radical generation in multiple systems, and ease of handling (it is crystalline at room temperature) has led to its adoption as the initiator of choice for lipid peroxidation studies. Since hyponitrites decompose to yield alkoxyl radicals, which are the initiating radicals when lipid hydroperoxides decompose, we reasoned that a lipophilic analog of DTBN may be more suitable for controlled initiation of lipid peroxidation in liposomes. Therefore, we synthesized di-*tert*-undecyl hyponitrite, hereafter DTUN (Figure 4A), by alkylation of silver hyponitrite with *tert*-undecyl iodide (see Supplemental Information for details, Figure S3A). DTUN was confirmed to be an efficient

initiator (see Figures S3B–S3D); the inhibition periods of PMC-inhibited autoxidations of 1-hexadecene yielded rates of radical initiation from which $ek_d = 8.3 \times 10^{-6}$ s^{-1} was derived—which was within experimental error of the value of 6.7×10^{-6} s^{-1} we found for DTBN. The value for MeOAMVN under the same conditions was measured to be 2.4×10^{-5} s^{-1}, in good agreement with the literature (Figure S3E) (Noguchi et al., 1998). In liposomes, $ek_d = 1.2 \times 10^{-6}$ s^{-1}, expectedly slower than in solution due to the increased microviscosity of the medium, and similar to that measured for MeOAMVN (1.0×10^{-6} s^{-1}) (Figures S3F and S3G). Interestingly, like MeOAMVN, DTBN was not efficiently incorporated into liposomes, because we found substantially less consumption of STY-BODIPY in DTBN-treated liposomes that were subsequently purified by SEC (see Figures S3H–S3J). In contrast, DTUN-treated liposomes oxidized to a similar extent before or after purification (Figure 4B). The rate constant for the decomposition of DTBN is too low to measure under our reaction conditions (Figure S3L). Addition of DTBN as an aliquot or before liposome extrusion results in immediate precipitation due to limited solubility in buffer. Previous experiments by Barclay et al., 1986 and Noguchi et al. (1998) were carried out in the presence of multilamellar (PLPC or DLPC) liposomes, where both DTBN and lipids were vortexed together in buffer to generate liposomes. This was likely done to ensure that the liposomes are formed around DTBN, effectively incorporating it into the lipid bilayer. However, this procedure results in multilamellar liposomes with a large polydispersity index, making standardization and reproduction of data very challenging.

DTUN-initiated co-autoxidations of STY-BODIPY and egg phosphatidylcholine were carried out initially with the same "training set" of compounds from Figures 3E and 3F under both chain and non-chain conditions (Figure 4C). In contrast to the results of the AAPH- and MeOAMVN-initiated autoxidations, the water-soluble RTAs did not inhibit autoxidation to a significant extent under either set of conditions. These results are similar to those obtained from MeOAMVN-initiated autoxidations carried out under chain conditions. Autoxidations under chain conditions, which require a large amount of lipid, are both expensive and more challenging to carry out due to the increased optical density of the solution, which lowers signal quality. Since the foregoing suggested that the RTA kinetics determined from the DTUN-initiated autoxidations are effectively independent of chain length (lipid concentration), we assayed the full test set of compounds in 1 mM PC liposomes. The addition of DTUN does not affect the liposomal particle size (see Figure S3K). The correlation of the k_{inh} values determined under these conditions and the EC_{50} values obtained in cells was excellent (Figure 4D, $R^2 = 0.84$).

The fact that DTUN-initiated autoxidations yield similar data at either high or low concentrations of lipid can be rationalized on the basis of available kinetic data (Figure 4E). Using PMC to illustrate this point, alkoxyl radicals abstract bis-allylic H-atoms with $k = 9.0 \times 10^6$ M^{-1} s^{-1}(Barclay et al., 1989), while they abstract an H-atom from PMC with $k = 1.1 \times 10^7$ M^{-1} s^{-1}. (The rate constant for reactions of PMC with alkoxyl radicals in phospholipid bilayers was estimated using the rate constant obtained in chlorobenzene from the following reference and the Ingold-Abraham equation [Equation 4], assuming the α_2^H of PMC = 0.38 and β_2^H of egg phosphatidylcholine of 0.79 (vide infra); Snelgrove et al., 2001.) Taking into account the relative concentration of PMC (4 μM) and polyunsaturated lipid (150 μM; linoleate makes up ca. 15% of the lipid in egg phosphatidylcholine, which is 1 mM), the kinetics predict that the DTUN-derived alkoxyl radicals will react with lipid 30-fold faster than with PMC.

H-Bonding of RTAs and Phospholipid Headgroups Attenuates Reactivity in a Predictive Fashion

The significant improvement in the cell potency versus RTA activity correlation observed when the kinetics were determined in liposomes instead of solution prompted us to consider the origin of this difference in more detail. We anticipated that it must be related to the dramatic suppression of reactivity observed upon moving from solution to liposomes, e.g., for PMC, $k_{inh} = 3.8 \times 10^6$ M^{-1} s^{-1} and 2.9×10^4 M^{-1} s^{-1} in chlorobenzene and egg PC liposomes, respectively. Although other suggestions have been made to account for this observation (*vide infra*), we hypothesized that H-bonding between the RTA and the phospholipid head group renders it unreactive to propagating lipid peroxyl radicals (Figure 5A).

Ingold has clearly shown that H-bonding can slow the rate of H-atom transfer reactions because, while engaged in an H-bond, the H-atom is inaccessible to abstraction by radical species (Figure 5B) (Litwinienko and Ingold, 2007; Snelgrove et al., 2001). Thus, the kinetics of H-atom transfer in H-bonding media follow a simple pre-dissociation model and can be expressed as in Equation 3 in Figure 5B. This expression is often shown as a linear free energy relationship, wherein the rate constant of the H-atom transfer in a given solvent ($k_{in\ h}^{S}$) is related to the rate constant in a non-H-bonding solvent ($k_{in\ h}^{0}$) by a term composed of the product of Abraham's H-bond acidity (α_2^H) (Abraham et al., 1989) and basicity (β_2^H) (Abraham et al., 1990) parameters of the H-atom donor and solvent, respectively (Equation 4) (Snelgrove et al., 2001).

The H-bond accepting ability of egg phosphatidylcholine was determined by the ^{19}F NMR method devised by Gurka and Taft (1969) (Equation 5, Figure S4A), who showed that the chemical shift difference between 4-fluorophenol and 4-fluoroanisole in a non-H-bonding solvent (e.g., CCl_4) is related to the formation constant of the H-bonded dimer between 4-fluorophenol and an added H-bond acceptor (Figure 5C). This can subsequently be recast in terms of β_2^H to facilitate comparison with other H-bond acceptors without needing to remeasure their individual equilibrium constants. The resultant value of is quite large—for comparison, $\beta_2^H = 0.38$ and 0.45 for water and an ester, respectively—the other possible H-bond acceptors in the liposome system. Moreover the determined β_2^H is consistent with that of a phosphate triester (0.77), as reported by Abraham et al. (1990). This value, when used with Equation 4 in Figure 5B, predicts a drop in k_{inh} for PMC ($\alpha_2^H = 0.38$) on going from chlorobenzene ($\beta_2^H = 0.09$) to egg PC bilayers ($\beta_2^H = 0.79$) of 161-fold, in very good agreement with the experimental observation of a 213-fold decrease in reactivity.

To demonstrate how profoundly the H-bonding interaction between an RTA and phospholipid head group can affect RTA kinetics, we explored the medium dependence of the reactivity

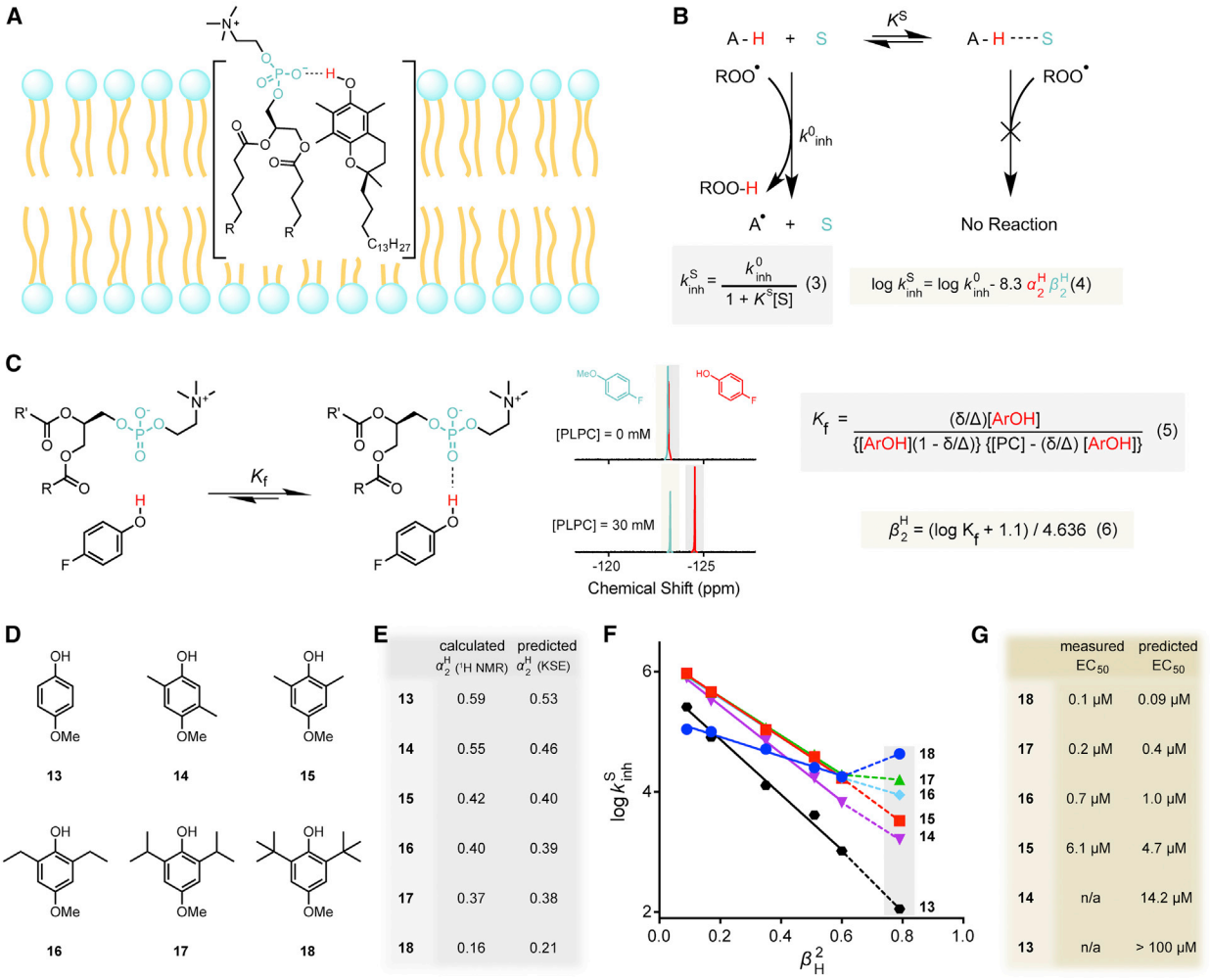

Figure 5. Hydrogen-Bonding Interactions Dramatically Suppresses the Reactivity of RTAs in Phospholipid Bilayers

(A) Formation of H-bonded complexes between α-tocopherol and the phosphatidylcholine head group are proposed to slow its reaction with peroxyl radicals in lipid bilayers.

(B) The equilibrium between "free" RTA (A–H) and RTA participating in a 1:1 hydrogen bond complex, with hydrogen bond accepting solvent S. Assuming the 1:1 complex does not react with peroxyl radicals, the kinetics of radical-trapping can be described as in Equations 3 or 4 (Snelgrove et al., 2001).

(C) The equilibrium between free 4-fluorophenol and 4-fluorophenol participating in a 1:1 hydrogen bond complex with the head group of phosphatidylcholine along with representative ^{19}F NMR spectra of 4-fluorophenol and 4-fluoroanisole (0.01 M) in CCl_4 in the presence of none (top) or 30 mM (bottom) egg PC used to derive β^H_2 of the phospholipid. Equations 5 and 6 can be used to determine the β^H_2, where A_0 is the concentration of 4-fluorophenol, B_0 is the concentration of egg PC, Δ is the difference in chemical shift seen between 4-fluorophenol and 4-fluoroanisole at a concentration of HBA saturation (B_0 = 0.20 M), and δ is the difference in chemical shift seen between 4-fluorophenol and 4-fluoroanisole at the dilute concentrations of egg PC.

(D and E) (D) Structures of differently substituted phenols along with their calculated (^{1}H NMR) and (E) predicted α^H_2 values.

(F) Correlation of $\log k^S_{inh}$ and β^H_2 for compounds **13** (●), **14** (▼), **15** (■), **16** (◆), **17** (▲), and **18** (●) in solvents with increasing hydrogen bond basicity.

(G) Predicted and measured EC_{50} values from RSL3-induced ferroptosis in Pfa1 MEFs for phenols **13**–**18**. Predicted EC_{50} values were obtained using the line of best fit from Figure 4C: $|\log EC_{50}| = 1.529\,(\log k_{inh}) - 0.0509$.

Data represent mean ± SD from three independent experiments. See also Figures S4 and S5.

of a group of structurally related phenols (Figure 5D) that differ slightly in their inherent H-atom transfer reactivity, but, due to differing steric environments of the reactive phenolic H-atom, exhibit substantial differences in their H-bond acidity (α^H_2 range from 0.59 to 0.16; Figure 5E; Figures S5A–S5I). All of the compounds are lipophilic with logP > 1.5 (the logP values for these compounds were estimated using the ChemDraw Chemical Properties Predictor to be: 1.5 (**13**), 2.5 (**14**), 2.5 (**15**), 3.3 (**16**), 4.0 (**17**), and 4.9 (**18**)), which ensures that the reactivity differences do not derive simply from different partitioning between the lipid and aqueous phases. The results are shown in Figure 5F (see Figure S4B for data).

The medium effects are dramatic—and clearly depend linearly on the β^H_2 of the solvent as predicted by Ingold (see Figure S4B).

Moreover, they clearly also depend on the H-bond donating ability of the phenol α_2^H. For example, while 4-methoxyphenol ($\alpha_2^H = 0.59$) and 2,6-dimethyl-4-methoxyphenol ($\alpha_2^H = 0.42$) differ in reactivity by a factor of ~3.5 in chlorobenzene, the difference in egg PC liposomes is nearly 30-fold. According to Equation 4, the slopes of the $\log k_{inh}/\beta_2^H$ correlations should correspond to $-8.3\alpha_2^H$. Indeed, we generally find good agreement between the α_2^H values derived from the slopes and the values we determined directly by NMR spectroscopy (Figure 5E), demonstrating the robustness of Ingold's relationship.

Interestingly, while the kinetic data obtained for the unhindered phenols **13**, **14**, and **15** in liposomes fall on the $\log k_{inh}/\beta_2^H$ correlation, as the bulk around the phenolic O-H increases further as in **16**, **17**, and **18**, the deviation from the correlation increases. Indeed, the most hindered phenol (**18**) is almost as reactive in the egg PC liposomes as in chlorobenzene—a stark difference from the dramatic drop in reactivity of the unhindered compounds in the different media (~3 orders of magnitude). This represents the limitation of this very useful linear free energy relationship: because the α_2^H of the phenols were determined using an unhindered H-bond acceptor (DMSO) and the β_2^H of PLPC was determined with an unhindered H-bond donor (4-fluorophenol), approximation of the H-bonding equilibrium between a hindered H-bond donor and a hindered H-bond acceptor is likely to be overestimated. Nevertheless, as expected based on the data in Figure 4C, the kinetics determined in liposomes using the DTUN initiator correctly predict the potency of these compounds in cells (Figure 5G; Figure S5J).

DISCUSSION

Lipid peroxidation has been implicated in disease pathogenesis for decades, but attempts to identify, design, or develop compounds to target aberrant lipid peroxidation for therapeutic or preventive purposes have largely failed. This has prompted many to believe that lipid peroxidation is not a part of disease etiology, but instead simply a hallmark of pathogenesis. Alternatively, it could be argued that the antioxidant compounds that have been the subject of the great multitude of clinical trials aimed at suppressing "radical damage," such as dietary (poly)phenols, were not good choices, simply convenient ones.

Lipids are the primary cellular target of radical damage due to both their high reactivity toward H-atom abstraction and their high local concentration in lipid bilayers, which facilitate propagation of the autoxidative chain reaction. Therefore, assessment of putative antioxidants should be made on the basis of their ability to compete with *lipids* for *peroxyl radicals* in *lipid bilayers*. Unfortunately, this is not common. Instead, surrogate experiments have been developed to assess antioxidant activity, such as the DPPH assay (Amorati and Valgimigli, 2018; Huang et al., 2005). Although the DPPH radical is isoelectronic with peroxyl radicals, the IC_{50} values obtained from this assay are clearly a poor predictor of the ability of a given compound to inhibit lipid peroxidation in cells (cf. Figure 1G). Indeed, in addition to being the wrong type of radical, the kinetics of H-atom transfer from the antioxidant to the radical are not determined; the IC_{50} values obtained from this assay simply reflect the position of the H-atom transfer equilibrium between DPPH and the test compound. The assay can be rendered more informative by determining the kinetics of the reaction, but this generally requires specialized equipment (a stopped-flow spectrophotometer) (Foti et al., 2008). Moreover, because these measurements are carried out in homogeneous solution, and the identity of the solvent can dramatically influence both the rates and the mechanism of the reaction (Litwinienko and Ingold, 2003, 2007), it is unlikely that the results will be predictive of what transpires in a cell or tissue.

Our recently implemented co-autoxidation approach using STY-BODIPY as a signal carrier served as an ideal starting point for the implementation of a far more predictive alternative antioxidant activity assay to DPPH (and presumably related existing methods, although this was not rigorously investigated). It should be pointed out that the assay can also be carried out with the commercially available C_{11}-BODIPY$^{581/591}$ cellular lipid peroxidation reporter (Drummen et al., 2002)—which served as the inspiration for the initial development of PBD-BODIPY—and which yields essentially indistinguishable results (see Supplemental Information for examples, Figures S2C, S2D, and S2F). Our efforts to generate a model system capable of predicting the potency of RTAs in cells highlights the importance of selecting both an appropriate reaction environment and an appropriate radical initiator. Indeed, the results of experiments initiated by MeOAMVN, the conventional choice as a lipid-soluble initiator, fail to provide a good correlation with cell-based results—yielding data which overestimate the reactivity of water-soluble or amphiphilic RTAs. This is a particularly significant problem at low concentrations of lipid, where there is no radical chain reaction, such that the added RTAs simply react with initiator-derived radicals (Figure 3G). When the concentration of lipid is increased such that a radical chain reaction takes place in the absence of RTA, uncertainty remains over the precise location of the somewhat amphiphilic—and not at all lipid-like—initiator. Therefore, some apparent inhibition of lipid peroxidation by water-soluble or amphiphilic RTAs may still derive simply from direct reactions with initiator-derived radicals. This is implied from the poor correlation of water-soluble RTA activity and anti-ferroptotic activity (Figure 3H).

The rate of consumption of STY-BODIPY (R_p) depends on the lipid concentration; it decreases with higher concentrations of lipid where the lipid competes with it for chain-propagating peroxyl radicals. This indirectly reports on the efficiency of initiation as the difference in R_p increases upon going from AAPH to MeOAMVN to DTUN. The ratios of R_p under chain to non-chain conditions are ~2, 7, and 8 for AAPH, MeOAMVN and DTUN, respectively. The newly developed lipophilic hyponitrite initiator DTUN addresses the shortcomings of the assay based upon MeOAMVN. The lengthy hydrocarbon side chains ensure that radical generation occurs exclusively in the lipid, and the greater reactivity of the alkoxyl radicals derived therefrom ensures they react with the lipids, which are in far greater abundance than the RTA (Figure 4E). Therefore, the inhibition observed in the presence of added RTAs—and apparent k_{inh} derived therefrom—results from their reaction with lipid peroxyl radicals. These advantages are clearly borne out in the excellent correlation between the $\log k_{inh}$ values determined using these conditions and the potency of the compounds in cells (Figure 4C). A further advantage of the use of DTUN to initiate lipid peroxidation is its mechanistic similarity to what presumably takes place

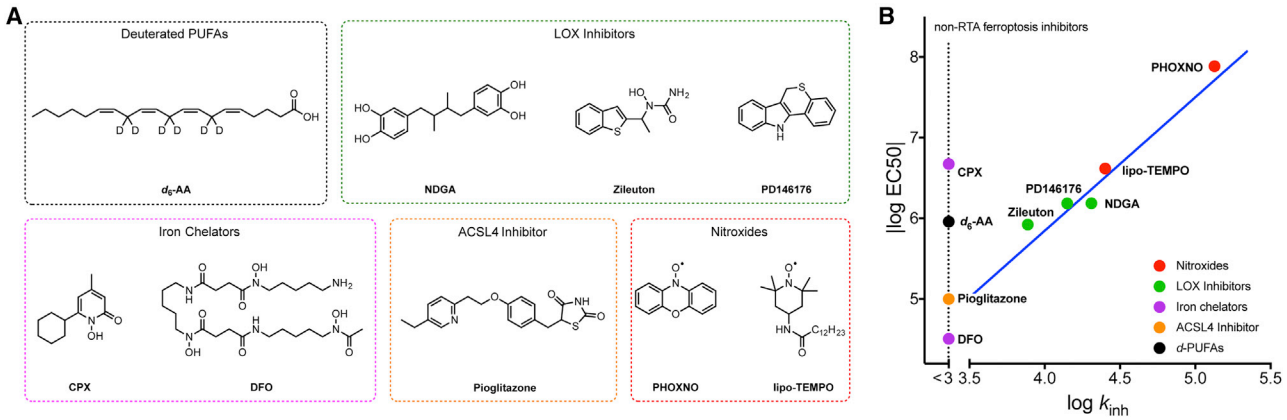

Figure 6. FENIX Resolves RTA and Non-RTA Inhibitors of Ferroptosis

(A) Structures of various classes of ferroptosis inhibitors and (B) their potency to inhibit RSL3-induced ferroptosis in Pfa1 MEFs and reactivity as inhibitors of lipid peroxidation overlaid on the correlation of EC_{50} and k_{inh} from Figure 4C. Compounds on the dotted line did not inhibit liposome autoxidation. Data represent mean ± SD from three independent experiments.

during ferroptosis, wherein (phospho)lipid hydroperoxides that escape detoxification by GPX4 can undergo Fenton-type reactions with low-valent iron (or other one-electron reductants). Although different in the structure of the alkyl side chains, the lipid-derived alkoxyl radicals that result are expected to have essentially identical reactivity to the alkoxyl radicals, which result from the decomposition of the hyponitrite.

In addition to offering a more rigorous high-throughput alternative to existing antioxidant activity assays, this approach enables researchers to reliably rule out RTA activity when attempting to elucidate the mode of action of compounds which protect against ferroptosis or related forms of oxidative cell death (e.g., oxytosis). A recent example that demonstrates this point relates to the role of lipoxygenase-catalyzed lipid peroxidation in ferroptosis. Lipoxygenases (LOXs) had been implicated in ferroptosis based largely upon the observation that LOX inhibitors are able to subvert ferroptosis. Characterization of the RTA activity of these LOX inhibitors enabled us to conclude that LOX activity could only sensitize cells to ferroptosis, since LOX inhibitors lacking RTA activity had no effect on cell survival—even in LOX-overexpressing cells (Shah et al., 2018). Indeed, when the k_{inh} is determined for these redox-active LOX inhibitors (NDGA, Zileuton, and PD146176) using the optimized assay protocol which afforded the EC_{50} versus logk_{inh} correlation in Figure 4, we find that these data also lie on the correlation (Figure 6)—fully consistent with our assertion that they protect cells from ferroptosis simply as RTAs (Shah et al., 2018). In addition to LOX inhibitors, we also assayed the nitroxides lipo-TEMPO and phenoxazine-*N*-oxyl (PHOXNO) (Griesser et al., 2018), since nitroxides have been suggested to inhibit ferroptosis via a mechanism involving mitochondrial ROS (Krainz et al., 2016). Again, we find these to be competent RTAs, with k_{inh} values that correlate with their potencies in cells, implying that they act merely as RTAs to prevent ferroptosis. In contrast, when other known ferroptosis inhibitors, such as the iron chelators desferrioxamine (DFO) and ciclopiroxamine (CPX), the deuterated polyunsaturated fatty acid d_6-arachidonic acid and a thiazolidinedione ACSL4 inhibitor, were assayed, no RTA activity could be detected, consistent with the fact that they act by other mechanisms.

At first glance, moving from homogeneous organic solution to lipid bilayers to assay RTA activity seems like an obvious and necessary step to obtain data that would be useful in predicting potency in cells. Barclay first quantitated the difference in the rate constants for the reaction between RTAs and peroxyl radicals upon moving from organic solution to lipid bilayers (Barclay et al., 1989, 1990, 1999). He, and others, generally attributed this observation to one of three factors: (1) the localization of the RTA, particularly its partitioning between the lipid and aqueous phase, (2) increased van der Waals interaction between aliphatic side chains on the RTA and the lipids, slowing their encounter with propagating radicals (Niki and Noguchi, 2004), and (3) H-bonding between the RTA and water at the lipid-aqueous interface. The importance of localization is abundantly clear from the low reactivity of water-soluble compounds (**2**, **3**, **5**, and **12**) toward lipid peroxyl radicals. The role of dynamics is evident upon comparing the reactivity of compounds that differ only in alkyl substitution, e.g., **1** and PMC: despite having similar reactivity in solution, PMC has a 2.6-fold higher reactivity in lipid bilayers than **1**. Although H-bonding between the RTA and water is insufficient to explain the drop in reactivity, we have now shown that H-bonding to the phospholipid head group is far stronger, and accounts for the massive drop in reactivity upon moving from solution to liposomes. These results highlight an element that is overlooked in the design of RTAs and/or anti-ferroptotic agents: H-bond acidity. Furthermore, it enables the prediction of the cytoprotective potencies of putative RTAs from the results of inhibited autoxidations or organic substrates in homogeneous organic solvents—no cell culture required! H-Bond acidity underlies the lackluster activity of phenols, the quintessential naturally derived antioxidants of much fanfare, as RTAs in a cellular context, and may contribute to the disappointing results of phenolic antioxidants in the many clinical trials in which they have been examined as potential therapeutic or preventive agents. Moreover, it underpins the identification of aromatic amines, such as Fer-1 (Dixon et al., 2012) and Lip-1 (Friedmann Angeli et al., 2014) in high-throughput screens of compound libraries for inhibitors of ferroptosis. Despite the fact that they are far less inherently

reactive than many phenols (including α-tocopherol), aromatic amines are simply far less H-bond acidic than phenols. It will be interesting to see how compounds which are excellent RTAs under relevant conditions (including cell models of ferroptosis) fare in clinical trials.

SIGNIFICANCE

Quantification of "antioxidant activity" is thought by many to be a routine experiment. However, investigators generally employ surrogate "antioxidant assays" which do not provide the kinetic information necessary to provide truly meaningful insight on the reactivity of putative antioxidants. Despite being the most popular of these assays by a considerable margin, the DPPH assay is not at all predictive of the potency of ferroptosis inhibitors – and should not be used to inform on radical-trapping antioxidant activity in cellular contexts. Instead, we show that the newly-developed fluorescence-enabled inhibited autoxidation (FENIX) assay is entirely predictive of cell potency. As such, results obtained from this assay can be used to provide insight on the mechanisms of ferroptosis modulators and which properties are important in the design of novel inhibitors of lipid peroxidation and/or ferroptosis. We expect this approach to be of very broad interest since the inhibition of lipid peroxidation is not only key to the inhibition of oxidative cell death, but also in various other pathological contexts. One of the key insights derived from the validation of FENIX is that phenols are, in general, relatively poor inhibitors of (phospho)lipid peroxidation, and that H-bonding between the phenol and the phospholipid headgroup is primarily responsible. This phenomenon may underlie the failure of the hundreds of clinical trials carried out with phenolic antioxidants.

STAR★METHODS

Detailed methods are provided in the online version of this paper and include the following:

- KEY RESOURCES TABLE
- LEAD CONTACT AND MATERIALS AVAILABILITY
- EXPERIMENTAL MODEL AND SUBJECT DETAILS
- METHOD DETAILS
  - DPPH Assay
  - Inhibited Autoxidation of 1-Hexadecene
  - Inhibited Autoxidation of Egg-PC Liposomes on UV-Vis
  - Inhibited Autoxidation of Egg-PC Liposomes on Plate Reader
  - Method to Calculate n and k_{inh}
  - Determination of α_2^H by ^{1}H NMR
  - Inhibition of Ferroptosis Induced by Gpx4 Inhibition with (1S,3R)-RSL3
  - Determination of Kinetic Chain Length
  - Determination of α_2^H by Kinetic Solvent Effect
  - Determination of β_2^H for PLPC by ^{19}F NMR
  - Synthesis and Characterization
- QUANTIFICATION AND STATISTICAL ANALYSIS
- DATA CODE AND AVAILABILITY

SUPPLEMENTAL INFORMATION

Supplemental Information can be found online at https://doi.org/10.1016/j.chembiol.2019.09.007.

ACKNOWLEDGMENTS

This work was supported by grants from the Natural Sciences and Engineering Research Council of Canada (NSERC) and the Canada Foundation for Innovation. R.S. and A.T.M.V.K. acknowledge NSERC for support via post-graduate and undergraduate scholarship programs, respectively.

AUTHOR CONTRIBUTIONS

D.A.P. designed and directed the research, and R.S., L.F., O.Z. performed the experimental work and contributed to project design. A.T.M.V.K. contributed preliminary experimental results. R.S., L.A.F., and D.A.P. wrote the manuscript.

DECLARATION OF INTERESTS

There are no competing interests.

Received: July 30, 2019
Revised: August 21, 2019
Accepted: September 9, 2019
Published: September 26, 2019

REFERENCES

Abraham, M.H., Grellier, P.L., Prior, D.V., Duce, P.P., Morris, J.J., and Taylor, P.J. (1989). Hydrogen bonding. Part 7. A scale of solute hydrogen-bond acidity based on log K values for complexation in tetrachloromethane. J. Chem. Soc. Perkin Trans. *2*, 699–711.

Abraham, M.H., Grellier, P.L., Prior, D.V., Morris, J.J., and Taylor, P.J. (1990). Hydrogen bonding. Part 10. A scale of solute hydrogen-bond basicity using log K values for complexation in tetrachloromethane. J. Chem. Soc. Perkin Trans. *2*, 521.

Amorati, R., and Valgimigli, L. (2015). Advantages and limitations of common testing methods for antioxidants. Free Radic. Res. *49*, 633–649.

Amorati, R., and Valgimigli, L. (2018). Methods to measure the antioxidant activity of phytochemicals and plant extracts. J. Agric. Food Chem. *66*, 3324–3329.

Barclay, L.R.C., Baskin, K.A., Locke, S.J., and Vinqvist, M.R. (1989). Absolute rate constants for lipid peroxidation and inhibition in model biomembranes. Can. J. Chem. *67*, 1366–1369.

Barclay, L.R.C., Baskin, K.A., Dakin, K.A., Locke, S.J., and Vinqvist, M.R. (1990). The antioxidant activities of phenolic antioxidants in free radical peroxidation of phospholipid membranes. Can. J. Chem. *68*, 2258–2269.

Barclay, L.R.C.C., Edwards, C.E., and Vinqvist, M.R. (1999). Media effects on antioxidant activities of phenols and catechols. J. Am. Chem. Soc. *99*, 6226–6231.

Barclay, L.R.C., Kong, D., and VanKessel, J. (1986). Autoxidation of phosphatidylcholines initiated with dicumylhyponitrite in solution and in bilayers. Can. J. Chem. *64*, 2103–2108.

Barnham, K.J., Masters, C.L., and Bush, A.I. (2004). Neurodegenerative diseases and oxidative stress. Nat. Rev. Drug Discov. *3*, 205–214.

Benzie, I.F.F., and Strain, J.J. (1996). The ferric reducing ability of plasma (FRAP) as a measure of "antioxidant power": the FRAP assay. Anal. Biochem. *239*, 70–76.

Blois, M.S. (1958). Antioxidant determinations by the use of a stable free radical. Nature *181*, 1199–1200.

Breslow, R., Groves, K., and Mayer, M.U. (2002). Antihydrophobic Cosolvent Effects for Alkylation Reactions in Water Solution, Particularly Oxygen versus Carbon Alkylations of Phenoxide Ions. J. Am. Chem. Soc. *124*, 3622–3635.

Burton, G.W., and Ingold, K.U. (1986). Vitamin-E—application of the principles of physical organic-chemistry to the exploration of its structure and function. Acc. Chem. Res. *19*, 194–201.

Cao, G., Alessio, H.M., and Cutler, R.G. (1993). Oxygen-radical absorbance capacity assay for antioxidants. Free Radic. Biol. Med. *14*, 303–311.

Chen, Z., Bertin, R., and Froldi, G. (2013). EC_{50} estimation of antioxidant activity in DPPH* assay using several statistical programs. Food Chem. *138*, 414–420.

Conrad, M., and Friedmann Angeli, J.P. (2015). Glutathione peroxidase 4 (Gpx4) and ferroptosis: what's so special about it? Mol. Cell. Oncol. *2*, e995047.

Cos, P., Hermans, N., Calomme, M., Maes, L., De Bruyne, T., Pieters, L., Vlietinck, A.J., and Vanden Berghe, D. (2003). Comparative study of eight well-known polyphenolic antioxidants. J. Pharm. Pharmacol. *55*, 1291–1297.

Denison, G.H., and Harle, O.L. (1949). Oxidation of lubricating oils at high temperatures. Ind. Eng. Chem. *41*, 934–937.

Di Paolo, G., and Kim, T.-W. (2011). Linking lipids to Alzheimer's disease: cholesterol and beyond. Nat. Rev. Neurosci. *12*, 284–296.

Dixon, S.J., Lemberg, K.M., Lamprecht, M.R., Skouta, R., Zaitsev, E.M., Gleason, C.E., Patel, D.N., Bauer, A.J., Cantley, A.M., Yang, W.S., et al. (2012). Ferroptosis: an iron-dependent form of nonapoptotic cell death. Cell *149*, 1060–1072.

Doll, S., Proneth, B., Tyurina, Y.Y., Panzilius, E., Kobayashi, S., Ingold, I., Irmler, M., Beckers, J., Aichler, M., Walch, A., et al. (2017). ACSL4 dictates ferroptosis sensitivity by shaping cellular lipid composition. Nat. Chem. Biol. *13*, 91–98.

Drummen, G.P.C., Van Liebergen, L.C.M., Op den Kamp, J.A.F., and Post, J.A. (2002). C11-BODIPY581/591, an oxidation-sensitive fluorescent lipid peroxidation probe: (micro)spectroscopic characterization and validation of methodology. Free Radic. Biol. Med. *33*, 473–490.

Dryzhakov, M., Hellal, M., Wolf, E., Falk, F.C., and Moran, J. (2015). Nitro-assisted Brønsted acid catalysis: application to a challenging catalytic azidation. J. Am. Chem. Soc. *137*, 9555–9558.

Finkel, T., and Holbrook, N.J. (2000). Oxidants, oxidative stress and the biology of ageing. Nature *408*, 239–247.

Foti, M.C. (2015). Use and abuse of the DPPH$^{\bullet}$ radical. J. Agric. Food Chem. *63*, 8765–8776.

Foti, M.C., Daquino, C., Mackie, I.D., DiLabio, G.A., and Ingold, K.U. (2008). Reaction of phenols with the 2,2-diphenyl-1-picrylhydrazyl radical. Kinetics and DFT calculations applied to determine ArO-H bond dissociation enthalpies and reaction mechanism. J. Org. Chem. *73*, 9270–9282.

Frank, C.E. (1950). Hydrocarbon autoxidation. Chem. Rev. *46*, 155–169.

Friedmann Angeli, J.P., Schneider, M., Proneth, B., Tyurina, Y.Y., Tyurin, V.A., Hammond, V.J., Herbach, N., Aichler, M., Walch, A., Eggenhofer, E., et al. (2014). Inactivation of the ferroptosis regulator Gpx4 triggers acute renal failure in mice. Nat. Cell Biol. *16*, 1180–1191.

Gao, M., Monian, P., Quadri, N., Ramasamy, R., and Jiang, X. (2015). Glutaminolysis and transferrin regulate ferroptosis. Mol. Cell *59*, 298–308.

Goldschmidt, S., and Renn, K. (1922). Zweiwertiger Stickstoff: Über das α, α-diphenyl-β-trinitrophenyl-hydrazyl. (IV. Mitteilung über Amin-Oxydation). Berichte Der Dtsch. Chem. Gesellschaft A B Ser. *55*, 628–643.

Gray, J.I. (1978). Measurement of lipid oxidation: a review. J. Am. Oil Chem. Soc. *55*, 539–546.

Griesser, M., Shah, R., Van Kessel, A.T., Zilka, O., Haidasz, E.A., and Pratt, D.A. (2018). The catalytic reaction of nitroxides with peroxyl radicals and its relevance to their cytoprotective properties. J. Am. Chem. Soc. *140*, 3798–3808.

Gurka, D., and Taft, R.W. (1969). Studies of hydrogen-bonded complex formation with p-fluorophenol. IV. The fluorine nuclear magnetic resonance method. J. Am. Chem. Soc. *91*, 4794–4801.

Haidasz, E.A., Van Kessel, A.T.M., and Pratt, D.A. (2016). A continuous visible light spectrophotometric approach to accurately determine the reactivity of radical-trapping antioxidants. J. Org. Chem. *81*, 737–744.

Huang, D., Boxin, O.U., and Prior, R.L. (2005). The chemistry behind antioxidant capacity assays. J. Agric. Food Chem. *53*, 1841–1856.

Ingold, K.U. (1961). Inhibition of the autoxidation of organic substances in the liquid phase. Chem. Rev. *61*, 563–589.

Ingold, K.U., and Pratt, D.A. (2014). Advances in radical-trapping antioxidant chemistry in the 21st century: a kinetics and mechanisms perspective. Chem. Rev. *114*, 9022–9046.

Kedare, S.B., and Singh, R.P. (2011). Genesis and development of DPPH method of antioxidant assay. J. Food Sci. Technol. *48*, 412–422.

Kigoshi, M., Sato, K., and Niki, E. (1993). Oxidation of lipids induced by dioctadecyl hyponitrite and di-t-butyl hyponitrite in organic solution and in aqueous dispersions. Effects of reaction medium and size of radicals on efficiency of chain initiation. Bull. Chem. Soc. Jpn. *66*, 2954–2959.

Krainz, T., Gaschler, M.M., Lim, C., Sacher, J.R., Stockwell, B.R., and Wipf, P. (2016). A mitochondrial-targeted nitroxide is a potent inhibitor of ferroptosis. ACS Cent. Sci. *2*, 653–659.

Krumova, K., Friedland, S., and Cosa, G. (2012). How lipid unsaturation, peroxyl radical partitioning, and chromanol lipophilic tail affect the antioxidant activity of α-tocopherol: direct visualization via high-throughput fluorescence studies conducted with fluorogenic α-tocopherol analogues. J. Am. Chem. Soc. *134*, 10102–10113.

Li, B., and Pratt, D.A. (2015). Methods for determining the efficacy of radical-trapping antioxidants. Free Radic. Biol. Med. *82*, 187–202.

Li, B., Harjani, J.R., Cormier, N.S., Madarati, H., Atkinson, J., Cosa, G., and Pratt, D.A. (2013). Besting vitamin E: sidechain substitution is key to the reactivity of naphthyridinol antioxidants in lipid bilayers. J. Am. Chem. Soc. *135*, 1394–1405.

Litwinienko, G., and Ingold, K.U. (2003). Abnormal solvent effects on hydrogen atom abstractions. 1. The reactions of phenols with 2,2-diphenyl-1-picrylhydrazyl (DPPH$^{\bullet}$) in alcohols. J. Org. Chem. *68*, 3433–3438.

Litwinienko, G., and Ingold, K.U. (2007). Solvent effects on the rates and mechanisms of reaction of phenols with free radicals. Acc. Chem. Res. *40*, 222–230.

Liu, Y., Wang, W., Li, Y., Xiao, Y., Cheng, J., and Jia, J. (2015). The 5-lipoxygenase inhibitor zileuton confers neuroprotection against glutamate oxidative damage by inhibiting ferroptosis. Biol. Pharm. Bull. *38*, 1234–1239.

Lonn, E. (2005). Effects of long-term vitamin E supplementation on cardiovascular events and cancer: a randomized controlled trial. J. Am. Med. Assoc. *293*, 1338–1347.

Magtanong, L., Ko, P.J., To, M., Cao, J.Y., Forcina, G.C., Tarangelo, A., Ward, C.C., Cho, K., Patti, G.J., Nomura, D.K., et al. (2019). Exogenous monounsaturated fatty acids promote a ferroptosis-resistant cell state. Cell Chem. Biol. *26*, 420–432.e9.

Matsuura, B.S., Keylor, M.H., Li, B., Lin, Y., Allison, S., Pratt, D.A., and Stephenson, C.R.J. (2015). A scalable biomimetic synthesis of resveratrol dimers and systematic evaluation of their antioxidant activities. Angew. Chem. Int. Ed. *54*, 3754–3757.

McIntyre, T.M., and Hazen, S.L. (2010). Lipid oxidation and cardiovascular disease: introduction to a review series. Circ. Res. *107*, 1167–1169.

Naidu, S.K., Klaus, E.E., and Duda, J.L. (1984). Evaluation of liquid phase oxidation products of ester and mineral oil lubricants. Ind. Eng. Chem. Prod. Res. Dev. *23*, 613–619.

Niki, E. (2010). Assessment of antioxidant capacity in vitro and in vivo. Free Radic. Biol. Med. *49*, 503–515.

Niki, E., and Noguchi, N. (2004). Dynamics of antioxidant action of vitamin E. Acc. Chem. Res. *37*, 45–51.

Noguchi, N., Yamashita, H., Gotoh, N., Yamamoto, Y., Numano, R., and Niki, E. (1998). 2,2'-Azobis (4-methoxy-2,4-dimethylvaleronitrile), a new lipid-soluble azo initiator: application to oxidations of lipids and low-density lipoprotein in solution and in aqueous dispersions. Free Radic. Biol. Med. *24*, 259–268.

Re, R., Pellegrini, N., Proteggente, A., Pannala, A., Yang, M., and Rice-Evans, C. (1999). Antioxidant activity applying an improved ABTS radical cation decolorization assay. Free Radic. Biol. Med. *26*, 1231–1237.

Ramirez, F., Chen, E.H., and Dershowitz, S. (1959). Reaction of Trialkyl Phosphites with p-Benzoquinone and with Other Symmetrically Substituted p-Quinones. A New Synthesis of Hydroquinone Monoalkyl Ethers. J. Am. Chem. Soc. *81*, 4338–4342.

Seibt, T.M., Proneth, B., and Conrad, M. (2019). Role of GPX4 in ferroptosis and its pharmacological implication. Free Radic. Biol. Med. *133*, 144–152.

Seiler, A., Schneider, M., Förster, H., Roth, S., Wirth, E.K., Culmsee, C., Plesnila, N., Kremmer, E., Rådmark, O., Wurst, W., et al. (2008). Glutathione peroxidase 4 senses and translates oxidative stress into 12/15-lipoxygenase dependent- and AIF-mediated cell death. Cell Metab. *8*, 237–248.

Semba, R.D., Ferrucci, L., Bartali, B., Urpí-Sarda, M., Zamora-Ros, R., Sun, K., Cherubini, A., Bandinelli, S., and Andres-Lacueva, C. (2014). Resveratrol levels and all-cause mortality in older community-dwelling adults. JAMA Intern. Med. *174*, 1077–1084.

Sesso, H.D., Christen, W.G., Bubes, V., Smith, J.P., MacFadyen, J., Schvartz, M., Manson, J.A.E., Glynn, R.J., Buring, J.E., and Gaziano, J.M. (2012). Multivitamins in the prevention of cardiovascular disease in men: the physicians' health study II randomized controlled trial. J. Am. Med. Assoc. *308*, 1751–1760.

Shah, R., and Pratt, D.A. (2016). Determination of key hydrocarbon autoxidation products by fluorescence. J. Org. Chem. *81*, 6649–6656.

Shah, R., Margison, K., and Pratt, D.A. (2017). The potency of diarylamine radical-trapping antioxidants as inhibitors of ferroptosis underscores the role of autoxidation in the mechanism of cell death. ACS Chem. Biol. *12*, 2538–2545.

Shah, R., Shchepinov, M.S., and Pratt, D.A. (2018). Resolving the role of lipoxygenases in the initiation and execution of ferroptosis. ACS Cent. Sci. *4*, 387–396.

Skouta, R., Dixon, S.J., Wang, J., Dunn, D.E., Orman, M., Shimada, K., Rosenberg, P.A., Lo, D.C., Weinberg, J.M., Linkermann, A., et al. (2014). Ferrostatins inhibit oxidative lipid damage and cell death in diverse disease models. J. Am. Chem. Soc. *136*, 4551–4556.

Snelgrove, D.W., Lusztyk, J., Banks, J.T., Mulder, P., and Ingold, K.U. (2001). Kinetic solvent effects on hydrogen-atom abstractions: reliable, quantitative predictions via a single empirical equation. J. Am. Chem. Soc. *123*, 469–477.

Stockwell, B.R., Friedmann Angeli, J.P., Bayir, H., Bush, A.I., Conrad, M., Dixon, S.J., Fulda, S., Gascón, S., Hatzios, S.K., Kagan, V.E., et al. (2017). Ferroptosis: a regulated cell death nexus linking metabolism, redox biology, and disease. Cell *171*, 273–285.

Viswanathan, V.S., Ryan, M.J., Dhruv, H.D., Gill, S., Eichhoff, O.M., Seashore-Ludlow, B., Kaffenberger, S.D., Eaton, J.K., Shimada, K., Aguirre, A.J., et al. (2017). Dependency of a therapy-resistant state of cancer cells on a lipid peroxidase pathway. Nature *547*, 453–457.

Weiwer, M., Bittker, J.A., Lewis, T.A., Shimada, K., Yang, W.S., MacPherson, L., Dandapani, S., Palmer, M., Stockwell, B.R., Schreiber, S.L., et al. (2012). Development of small-molecule probes that selectively kill cells induced to express mutant RAS. Bioorg. Med. Chem. Lett. *22*, 1822–1826.

Xie, J., and Schaich, K.M. (2014). Re-evaluation of the 2,2-diphenyl-1-picrylhydrazyl free radical (DPPH) assay for antioxidant activity. J. Agric. Food Chem. *62*, 4251–4260.

Yang, W.S., and Stockwell, B.R. (2008). Synthetic lethal screening identifies compounds activating iron-dependent, nonapoptotic cell death in oncogenic-RAS-harboring cancer cells. Chem. Biol. *15*, 234–245.

Yin, H., Xu, L., and Porter, N.A. (2011). Free radical lipid peroxidation: mechanisms and analysis. Chem. Rev. *111*, 5944–5972.

Zhao, W., Huang, L., Guan, Y., and Wulff, W.D. (2014). Three Component Asymmetric Catalytic Ugi Reaction – Concinnity from Diversity via Substrate Mediated Catalyst Assembly. Angew. Chem. Intl. Ed. *53*, 3436–3441.

Zilka, O., Shah, R., Li, B., Friedmann Angeli, J.P., Griesser, M., Conrad, M., and Pratt, D.A. (2017). On the mechanism of cytoprotection by ferrostatin-1 and liproxstatin-1 and the role of lipid peroxidation in ferroptotic cell death. ACS Cent. Sci. *3*, 232–243.

Zielinski, Z.A.M., and Pratt, D.A. (2017). Lipid peroxidation: kinetics, mechanisms, and products. J. Org. Chem. *82*, 2817–2825.

Zielinski, Z.A.M., and Pratt, D.A. (2019). H-atom abstraction vs. addition: accounting for the diverse product distribution in the autoxidation of cholesterol & its esters. J. Am. Chem. Soc. *141*, 3037–3051.

STAR★METHODS

KEY RESOURCES TABLE

REAGENT or RESOURCE	SOURCE	IDENTIFIER
Chemicals, Peptides, and Recombinant Proteins		
DPPH (2,2,-diphernyl-1-picrylhydrazine)	Sigma-Aldrich	D9132; CAS: 1898-66-4
α-tocopherol	Sigma-Aldrich	258024; CAS: 10191-41-0
PMC (2,2,5,7,8-pentamethyl-6-chromanol)	Sigma-Aldrich	430676; CAS: 950-99-2
Ascorbic acid	Sigma-Aldrich	A5960; CAS: 50-81-7
Glutathione (reduced form)	Sigma-Aldrich	PHR1359; CAS: 70-18-8
Resveratrol	Sigma-Aldrich	R5010; CAS: 501-36-0
NADH disodium salt (reduced form)	Sigma-Aldrich	10128023001; CAS: 606-68-8 (anhydrous)
EGCG	Cayman Chemical	70935; CAS: 989-51-5
Curcumin	Sigma-Aldrich	C1386; CAS: 458-37-7
Di-*tert*-butylresveratrol	Reference (Matsuura et al., 2015)	N/A
3,5-Di-*tert*-butylcatechol	Sigma-Aldrich	D45800; CAS: 1020-31-1
2,5-Di-*tert*-butylhydroquinone	Sigma-Aldrich	112976; CAS: 88-58-4
C_{15}-THN	Reference (Li et al., 2013)	N/A
NAC (N-acetyl-L-cysteine)	Sigma-Aldrich	A7250; CAS: 616-91-1
Liproxstatin-1	Reference (Friedmann Angeli et al., 2014)	Lip-1
Ferrostatin-1	Reference (Skouta et al., 2014)	Fer-1
STY-BODIPY	Reference (Haidasz et al., 2016)	STY-BODIPY
PBD-BODIPY	Reference (Haidasz et al., 2016)	PBD-BODIPY
AAPH (2,2'-azobis(2-amidinopropane) dihydrochloride)	Sigma-Aldrich	440914; CAS: 2997-92-4
MeOAMVN (2,2'-azobis(4-methoxy-2,4-dimethylvaleronitrile)	Wako Pure Chemical Corporation	CAS: 15545-97-8
DTUN	This paper	N/A
4-hydroxyanisole	Sigma-Aldrich	M18655; CAS: 150-76-5
2,5-Dimethyl-4-methoxyphenol	Reference (Breslow et al., 2002; Ramirez et al., 1959; Zhao et al., 2014)	N/A
2,6-Dimethyl-4-methoxyphenol	Reference (Breslow et al., 2002; Ramirez et al., 1959; Zhao et al., 2014)	N/A
2,6-Diethyl-4-methoxyphenol	This paper	N/A
2,6-Diisopropyl-4-methoxyphenol	This paper	N/A
2,6-Di-*tert*-butyl-4-methoxyphenol	Sigma-Aldrich	251062; CAS: 489-01-0
d_6-arachidonic acid	Gift from Mikhail S. Shchepinov (Retrotope, Inc.)	N/A
NDGA	Cayman Chemical	70300; CAS: 500-38-9
Zileuton	Cayman Chemical	10006976; CAS: 111406-87-2
PD146176	Cayman Chemical	10010518; CAS: 4079-26-9
CPX (ciclopirox olamine)	Sigma-Aldrich	C2162700; CAS: 41621-49-2
DFO (deferoxamine mesylate salt)	Sigma-Aldrich	D9533; CAS: 138-14-7
Pioglitazone	Cayman Chemical	71745; CAS: 111025-46-8
PHOXN (Phenoxazine)	Sigma-Aldrich	263893; CAS: 135-67-1
lipo-TEMPO	Reference (Griesser et al., 2018)	N/A
DHQN	Reference (Zilka et al., 2017)	N/A
PHOXNO	Reference (Griesser et al., 2018)	N/A
Arylamines (S1-S12)	Reference (Shah et al., 2017)	N/A
(*1S*,*3R*)-RSL3	Reference (Friedmann Angeli et al., 2014; Skouta et al., 2014)	RSL3

(*Continued on next page*)

Continued

REAGENT or RESOURCE	SOURCE	IDENTIFIER
Experimental Models: Cell lines		
Pfa1 cells	Reference (Friedmann Angeli et al., 2014; Seiler et al., 2008)	N/A
Software and Algorithms		
ChemDraw Ultra, Version 14.0	Perkin Elmer	http://www.perkinelmer.com/category/chemdraw
Prism, Version 7.0	GraphPad Software	https://www.graphpad.com/scientific-software/prism/
BioTek Gen5.1	BioTek Synergy H1 Software	https://www.biotek.com/products/software-robotics-software/gen5-microplate-reader-and-imager-software/

LEAD CONTACT AND MATERIALS AVAILABILITY

Further information and requests for resources and reagents should be directed to and will be fulfilled by the Lead Contact Derek A. Pratt (dpratt@uottawa.ca).

EXPERIMENTAL MODEL AND SUBJECT DETAILS

Pfa1 cells were generated as described in (Seiler et al., 2008) and shared by the laboratory of Dr. Marcus Conrad. Pfa1 cells were cultured at 37°C in a 5% CO_2 atmosphere unless otherwise indicated. Pfa1 cells were cultured in DMEM with 10% FBS, 1% 100× non-essential amino acid solution, 1 mM sodium pyruvate and 1% penicillin-streptomycin. Cells were passaged by dissociation with 0.05% trypsin and 0.2% EDTA every two days and reseeded at a dilution of 1:20. All cell experiments were carried out as a minimum of three biological replicates.

METHOD DETAILS

DPPH Assay

Test compounds (or vehicle) at various concentrations were dissolved in ethanol and added to clear bottom 96-well plates. To this was added a solution of DPPH dissolved in ethanol to achieve a final concentration of 100 μM. Samples were placed in the BioTek Synergy H1 plate reader and mixed vigorously for 60 s. The samples were incubated at room temperature for 30 min and the absorbance at 517 nm was measured (Cos et al., 2003). Samples were subtracted for background (ethanol only) and normalized to starting DPPH absorbance. The IC_{50} values were obtained by fitting the results to a dose-response curve in GraphPad Prism. The results represent the mean ± S.E. of three independent experiments.

Inhibited Autoxidation of 1-Hexadecene

A 3.5-mL quartz cuvette was charged with PhCl (0.44 mL), 1-hexadecene (2.00 mL). The cuvette was preheated to 37°C in a thermostatted sample holder of a UV-vis spectrophotometer and allowed to equilibrate for approximately 15 min. To the cuvette was added PBD- BODIPY (12.5 μL of a 2.00 mM stock solution in 1,2,4-trichlorobenzene) and AIBN (50 μL of a 300 mM stock solution in chlorobenzene). The solution was thoroughly mixed prior to monitoring the uninhibited co-autoxidation via the disappearance of the PBD-BODIPY probe at 588 nm for 10 min to ensure the reaction was proceeding at a constant rate. Finally, the antioxidant under investigation was added (10.0 μL of a 1.0 mM solution in chlorobenzene), the solution was mixed thoroughly, and the absorbance readings were resumed. The resulting Abs vs time data were processed as previously reported (Haidasz et al., 2016). The rate of initiation ($R_i = 1.3 \times 10^{-9}$ M s^{-1}) and second order rate constant for propagation for the dye ($k_{PBD\text{-}BODIPY} = 3792$ M^{-1} s^{-1}) necessary to compute stoichiometric data (n) and inhibition rate constants (k_{inh}) were determined using PMC as a standard, which has an established stoichiometry of 2.

Inhibited Autoxidation of Egg-PC Liposomes on UV-Vis

To a cuvette of 2.34 mL of 10 mM PBS at pH 7.4 was added liposomes (125 μL of 20 mM stock in PBS at pH 7.4) and the solution was equilibrated for 5 minutes at 37°C (liposome formation from egg PC was described elsewhere).(Li et al., 2013) The cuvette was blanked and 10 μL of 2 mM STY-BODIPY in DMSO was added followed by 10 μL of 0.05 M MeOAMVN in acetonitrile and the solution was thoroughly mixed. After 5 minutes, an aliquot of RTA stock solution in DMSO was added and the loss of absorbance at 565 nm followed. The inhibition rate constant (k_{inh}) and stoichiometry (n) was determined for each experiment according to Equations S2 and S1, respectively. The resulting Abs vs time data were processed as previously reported (Haidasz et al., 2016). The rate of initiation ($R_i = 2.5 \times 10^{-9}$ M s^{-1}) and second order rate constant for propagation for the dye ($k_{STY\text{-}BODIPY} = 894$ M^{-1} s^{-1}) necessary to compute

stoichiometric data (n) and inhibition rate constants (k_{inh}) were determined using PMC as a standard, which has an established stoichiometry of 2. Kinetic data are given as averages of three independent measurements.

Inhibited Autoxidation of Egg-PC Liposomes on Plate Reader

To a black 96-well polypropylene plate (Nunc), was added a solution containing liposomes (1 mM for non-chain; 20 mM for chain conditions) and either one of STY-BODIPY (1 μM) or C_{11}-BODIPY (1 μM) in PBS at pH 7.4 to a final volume of 295 μL (It is suggested to make a larger volume in falcon tube, pre-mix and aliquot 295 μL to each well). For liposome generation from eggPC please see: (Li et al., 2013). This was followed by the addition of inhibitors (2 μL aliquots) at desired concentrations to the appropriate wells. The plate was incubated for 10 minutes at 37°C in the BioTek Synergy H1 plate reader followed by a vigorous mixing protocol for 5 minutes. The plate was ejected from the plate reader and the autoxidation was initiated by the addition of a 3 μL aliquot of either AAPH (1 mM in PBS at pH 7.4), MeOAMVN (0.2 mM in MeCN) or DTUN (0.2 mM in EtOH), followed by another mixing protocol for 5 minutes. The plate was incubated for an additional 10 minutes to equilibrate at 37°C before data was acquired by excitation of the probes at 488 nm and emission was measured at 518 nm (gain: 70). The data was transformed by diving the raw RFU values by the response factor of 7.49×10^4 RFU/μM or 1.93×10^4 RFU/μM for STY-BODIPY and C11-BODIPY, respectively. The data shown is an average of three independent experiments. Settings such as read intervals and gain must be optimized for each instrument. Prior to the first set of experiments, the response factor must be measured for chain and non-chain conditions by carrying out a set of uninhibited autoxidations with varying concentrations of the probe (0.2, 0.4, 0.6, 0.8, 1 μM); see Figures S2A–S2D. The response factor varies depending on the instrument and the settings being utilized. Once determined, the same response factor can then be used to transform the data and does not need to be measured again. The inhibition rate constant (k_{inh}) and stoichiometry (n) can be determined for each experiment according to Equations S2 and S1, respectively (see example of a calculation below). The second order rate constant for propagation for the dye is $k_{STY\text{-}BODIPY} = 894\ M^{-1}\ s^{-1}$ for non-chain and $k_{STY\text{-}BODIPY} = 1703\ M^{-1}\ s^{-1}$ for chain; $k_{C11\text{-}BODIPY} = 2000\ M^{-1}\ s^{-1}$ for non-chain conditions. The rate of initiation (R_i) necessary to compute stoichiometric data (n) and inhibition rate constants (k_{inh}) were determined using PMC as a standard, which has an established stoichiometry of 2.

Method to Calculate n and k_{inh}

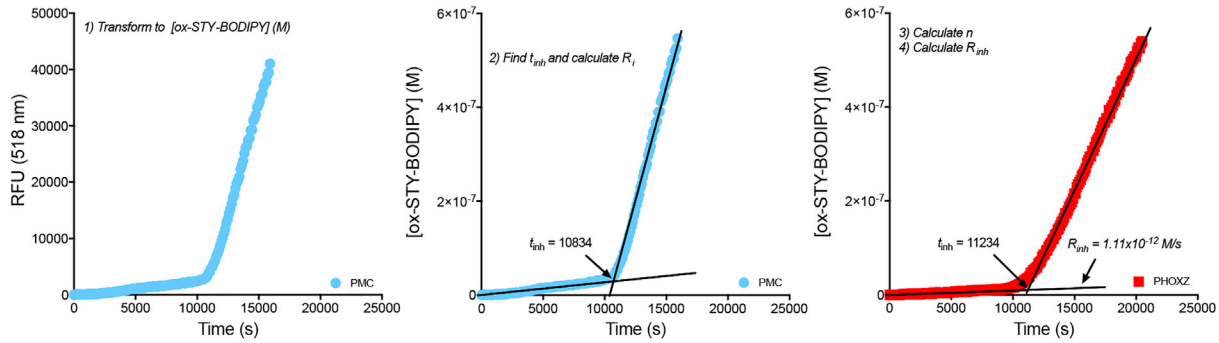

Variables

$k_{STY-BODIPY} = 894\ M^{-1}s^{-1}$ (non-chain)
[STY−BODIPY] = dye concentration at t = 0 (M)
n = stoichiometry
R_i = calculated as shown
[RTA] = antioxidant concentration (M)
R_{inh} = rate of inhibition, (M/s)
t_{inh} = inhibition time (s)
[RTA] = antioxidant concentration (M)

1) Covert all RFU into [ox-STY-BODIPY] $\left([ox - STY - BODIPY] = \dfrac{RFU}{7.5 \times \dfrac{10^{10} RFU}{M}} \right)$

2) Calculate the rate of initiation $\left(R_i = \dfrac{[RTA] \cdot n}{t_{inh}} \right)$ by standardizing using PMC

[PMC] = 4μM, n = 2, t_{inh} = time of inhibition = 10885 s $\therefore R_i = \dfrac{[4 \times 10^{-6} M] \cdot 2.0}{10885} = 7.40 \times 10^{-10}\ s^{-1}$

3) Calculate stoichiometry using Equation S1

$$\left(n = \frac{t_{inh} \cdot R_i}{[RTA]}\right) \quad \text{(Equation S1)}$$

for PHOXZ, t_{inh} = 11234 s $\therefore n = \frac{11234 \cdot 7.40 \times 10^{-10}}{[4 \times 10^{-6} M]} = 2.1$

4) Determine R_{inh} from the rate of change of the inhibited period
for PHOXZ R_{inh} = 1.11x10^{-12}M/s

5) Calculate k_{inh} using rearranged Equation S2

$$\left(k_{inh} = -\frac{k_{STY-BODIPY} \cdot [STY - BODIPY] \cdot R_i}{n \cdot [RTA] \cdot R_{inh}}\right) \quad \text{(Equation S2)}$$

For PHOXZ $\therefore k_{inh} = -\frac{894 M^{-1}s^{-1} \cdot [1 \times 10^{-6} M] \cdot 7.40 \times 10^{-10} s^{-1}}{2.1 \cdot [4 \times 10^{-6} M] \cdot 1.11 \times 10^{-12} M s^{-1}} = 7.1\text{x}10^4 \text{M}^{-1}\text{s}^{-1}$

Determination of α_2^H by ^{1}H NMR

Functional groups which engage significantly as hydrogen bond donors (having measurable α_2^H values) demonstrate substantially lower-field chemical shifts in a strongly hydrogen bonding solvent (DMSO-d_6) compared to a weakly hydrogen bonding solvent ($CDCl_3$ or Benzene-d_6). The correlation between α_2^H values and the $\Delta\delta$ of DMSO-d_6 and $CDCl_3$ was described by Abraham et al. to afford the empirical relationship Equation S3. In a previously published paper we utilized benzene-d_6 instead of $CDCl_3$ (due to an unusual incompatibility between $CDCl_3$ and several of our phenoxazines/phenothiazines) which afforded a similar correlation rendering Equation S4.

$$\alpha_2^H = 0.133\Delta\delta_{DMSO-CDCl3} + 0.0066 \quad \text{(Equation S3)}$$

$$\alpha_2^H = 0.134\Delta\delta_{DMSO-Ben} - 0.1087 \quad \text{(Equation S4)}$$

Inhibition of Ferroptosis Induced by Gpx4 Inhibition with (1S,3R)-RSL3

Pfa1 cells (3,000 in 100 μL) were seeded in 96-well plates and cultured overnight. The next day the media was removed, the cells were washed twice with PBS and the cells were suspended in new media for 30 minutes before addition of RTAs and LOX inhibitors. Ferroptosis was induced using (*1S*, *3R*)-RSL3 (10 μM) 30 minutes after incubation of compounds. Cell viability was assessed 6 hours later using the AquaBluer assay (MultiTarget Pharmaceuticals, LLC) according to the manufacturer's instructions. Cell viability was calculated by normalizing the data to untreated controls. Experiments are carried out with six-technical replicates (n = 6 wells of a 96-well plate) and performed independently with a minimum of three biological replicates.

Determination of Kinetic Chain Length

$$\text{Kinetic Chain Length} = \frac{R_p}{R_i} \times \frac{k_p[substrate]}{k_p[Dye]}$$

$$\text{Non} - \text{chain conditions (AAPH)} = \frac{\frac{5.1 \times 10^{-11} M}{s}}{\frac{5.8 \times 10^{-10} M}{s}} \times \frac{62\, M^{-1}s^{-1}\left[1.5 \times 10^{-4} M\right]}{894\, M^{-1}s^{-1}\left[1.0 \times 10^{-6} M\right]}$$

$$\text{Chain conditions (AAPH)} = \frac{\frac{3.3 \times 10^{-11} M}{s}}{\frac{4.6 \times 10^{-10} M}{s}} \times \frac{62\, M^{-1}s^{-1}\left[3.0 \times 10^{-3} M\right]}{1703\, M^{-1}s^{-1}\left[1.0 \times 10^{-6} M\right]}$$

Determination of α_2^H by Kinetic Solvent Effect

Utilizing the Ingold-Abraham relationship (Equation S5) in the form of Equation S6, α_2^H is determined as the intercept of Equation S7

$$logk_{inh}^{0} = logk_{inh}^{S} + 8.3\alpha_2^H\beta_2^H \quad \text{(Equation S5)}$$

$$logk_{inh}^{PhCl} + 8.3\alpha_2^H\beta_2^{H(PhCl)} = logk_{inh}^{S} + 8.3\alpha_2^H\beta_2^{H(S)} \quad \text{(Equation S6)}$$

$$\frac{logk_{inh}^{PhCl}}{8.3\left(\beta_2^{H(S)} - \beta_2^{H(PhCl)}\right)} = \frac{logk_{inh}^{S}}{8.3\left(\beta_2^{H(S)} - \beta_2^{H(PhCl)}\right)} + \alpha_2^H \quad \text{(Equation S7)}$$

Determination of β_2^H for PLPC by ^{19}F NMR

The H-bond accepting solute (PLPC) was diluted in CCl_4 to render five dilute solutions of differing concentrations and one 0.20M solution. To these were added 4-fluorophenol and 4-fluoroanisole for a final concentration of 0.01M of each. The solutions were transferred into NMR tubes containing seal capillaries of benzene-d6 with α,α,α-trifluorotoluene, after which their ^{19}F spectra were recorded with a Bruker Avance II 300 equipped with a thermostat (sample kept at 37°C). The 1:1 H-bond formation constant (K_f) of 4-fluorophenol and the H-bond acceptor(s) can be determined with by Equation S8 as described by Taft and co-workers:

$$K_f = \frac{\left(\frac{\delta}{\Delta}\right)A_0}{\left\{A_0\left[1 - \left(\frac{\delta}{\Delta}\right)\right]\right\}\left[B_0 - \left(\frac{\delta}{\Delta}\right)A_0\right]} \quad \text{(Equation S8)}$$

Where A_0 is the concentration of 4-fluorophenol, B_0 is the concentration of the H-bond acceptor (PLPC), Δ is the difference in chemical shift between 4-fluorophenol and 4-fluoroanisole sufficient to saturate H-bonding with 4-fluorophenol (maximum δ, [PLPC] = 0.20M), and δ is the observed difference in chemical shift between 4-fluorophenol and 4-fluoroanisole at the corresponding B_0 and A_0. The β_2^H can be calculated from the measured K_f using Equation S9.

$$\beta_2^H = \frac{(logK_f + 1.1)}{4.636} \quad \text{(Equation S9)}$$

Synthesis and Characterization

Synthesis of DTUN

2-Methyldecan-2-ol. 1-Bromooctane (19.3 g, 100 mmol, 1 eq) was added dropwise to magnesium turnings (3.04 g, 125 mmol, 1.25 eq, activated dry with iodine) suspended in anhydrous THF (100 mL) under N_2 atmosphere at a rate that maintained a gentle reflux. Upon completion of the reaction, the solution was transferred via cannula to a dry RBF under N_2, cooled thoroughly in an ice bath, and acetone (7.0 mL, 95 mmol, 0.95 eq, dried overnight on 3A sieves) was added dropwise over about 30 min. The mixture was allowed to warm to room temperature over 3 h, then recooled on ice, quenched with 6 mL acetic acid and concentrated *in vacuo*. The residue was vigorously stirred with 100 mL 3:1 chloroform:isopropanol and 100 mL water for 10 min before extracting the aqueous layer 2x 50 mL 3:1 chloroform:isopropanol. The combined organics were washed 3x 100mL 10% aqueous sodium chloride, 1x 100 mL brine, dried over Na_2SO_4, filtered and concentrated to dryness. The residual oil was distilled with a short path fractionating distillation apparatus collecting the middle fraction of distillate to afford 2-methyldecan-2-ol (13.95 g, 81%) as a colourless oil. Spectra were in agreement with literature values.(Dryzhakov et al., 2015).

2-Iodo-2-methyldecane. An oven dried 25 mL round-bottom flask and stir bar were cooled under N_2 atmosphere, wrapped completely in foil, charged with concentrated HI (6.7 mL, *ca*. 2 eq) and then cooled in an ice bath. Lithium iodide (3.36g, 25 mmol, 1 eq) was added in portions (caution: exotherm/fumes with powdered LiI; beads are preferred). A solution of 2-methyldecan-2-ol (4.31 g, 25 mmol, 1 eq.) in methylene chloride (5 mL) was added slowly by syringe with vigorous stirring under nitrogen atmosphere. The ice bath was then removed and the biphasic mixture stirred for about 10 minutes, at which point the alcohol was completely consumed by ^{1}H NMR. The mixture was carefully transferred to separatory funnel and the bottom aqueous layer cautiously extracted twice with methylene chloride (10 mL). The combined organic layers were washed once with 1:1 brine:water containing drops of sodium bisulfite solution until the mixture was mostly colourless. The organic extracts were fully protected from light while drying over Na_2SO_4, filtering and concentrating on a rotary evaporator followed by hivac (flask backfilled with nitrogen) to yield the title compound as a pale oil (6.63 g, 94%). The product was pure by ^{1}H NMR without distillation and was stored at -20°C in a foil-wrapped vial, ideally backfilled with nitrogen. ^{1}H NMR (300 MHz, $CDCl_3$) δ 1.92 (m, 6H), 1.65-1.22 (m, 14H), 0.88 (t, J = 6.9 Hz, 3H). ^{13}C NMR (75 MHz, $CDCl_3$) δ 53.27, 50.72, 38.20, 32.02, 29.65, 29.57, 29.43, 28.63, 22.81, 14.27. HRMS: m/z Calc: $C_{11}H_{23}$ (ESI: M-I)$^+$ 155.1800 Found: 155.1817.

*Di-tert-undecyl Hyponitrite (**DTUN**)*. An oven dried 25 mL round-bottom flask and stir bar were cooled under N_2 atmosphere and charged with 2-iodo-2-methyldecane (1.44g, 6 mmol) followed by degassed anhydrous methylene chloride (10 mL). The flask was completely wrapped in aluminum foil to exclude light and then cooled thoroughly in an ice bath. Freshly dried silver hyponitrite (1.24 g, 4.5 mmol) was added in three portions over 5 min with vigorous stirring. The ice bath was then removed and NMR analysis indicated consumption of the tertiary iodide usually within 10-20 min. The reaction mixture was then re-cooled in an ice bath and diluted with cold pentane (10 mL) before filtering over celite. The filtrate was concentrated on a rotary evaporator without heating followed by hivac for about 5 min while on ice. The residual oil was crystallized overnight from methanol (*ca*. 20 mL, N_2 purged) on dry ice. The majority of supernatant was then removed by syringe, discarded, and the solid washed with three portions of cold methanol in the same manner. The solid was allowed to thaw into a small volume of methanol (*ca*. 5 mL) until a solution formed. The product was promptly isolated thereafter while being kept cold on ice at all times. The solution was extracted with three portions of cold pentane (5 mL), the combined pentane extracts washed once with 1:1 methanol:water, dried over Na_2SO_4, filtered, concentrated on a rotary evaporator without heating followed by high vacuum to yield **DTUN** (270 mg, 24%) as a colourless wax. The product when free from residual solvent is solid on ice and rapidly melts when allowed to warm to ambient temperature. The solid was aliquoted by Pasteur pipette into tared vials and the vials were stored at -78°C. Stocks up to 0.2 M were prepared in ethanol or chlorobenzene and held on ice or dry ice just prior to use. ^{1}H NMR (600 MHz, $CDCl_3$) δ 1.65 (m, 2H), 1.34 (s, 6H), 1.34-1.24 (m, 12H), 0.88 (t, J = 6.6 Hz, 3H). ^{13}C NMR (151 MHz, $CDCl_3$) δ 83.42, 40.63, 32.03, 30.16, 29.69, 29.42, 25.94, 24.02, 22.82, 14.27. FTIR (ATR) ν: 988, 1147, 1368, 1384, 1466, 2854, 2923 cm^{-1}. HRMS: m/z Calc: $C_{11}H_{23}$ (EI: M-$C_{11}H_{23}N_2O_2$)$^+$ 155.1794 Found: 155.1787.

Synthesis of Phenols

2,6-Diethylhydroquinone. A 100mL double neck round bottom flask was charged with glacial acetic acid (35mL), concentrated sulfuric acid (0.4 mL) and 2,6-diethylphenol (3.89g; 25.9mmol). With mixing, 30% H_2O_2 (13mL) was add by dropping funnel. While monitoring the temperature of the solution with an alcohol thermometer (affixed through side neck) the mixture was gradually heated to 50°C (heat gun) after which the reaction was sufficiently exothermic to maintain its temperature. The reaction was kept between 55 and 65°C for ~30 minutes after which the heat of the reaction subsided until cooling to room temperature. The reaction was poured into water and extracted with ethyl acetate three times. The combined organic extracts were rinsed three times with 1M NaOH solution, and subsequently dried with $MgSO_4$, filtered, and concentrated under reduced pressure. The residue was dissolved into ether (40mL) and transferred to a 250mL round bottom flask charged with methanol (25mL), water (90mL), and sodium dithionite (13g). The flask was sealed, evacuated, and backfilled with N_2 and left to stir overnight. The ether was then separated, and the aqueous phases was extracted with ether. The combined organic solutions were subsequently dried with $MgSO_4$, filtered, and concentrated under reduced pressure. The product was isolated by column chromatography (30% EtOAc in hexanes) and recrystallized out of hexanes affording 2,6-diethylhydroquinone as white needles (1.00g, 23.2%); mp 90-92°C; ^{1}H NMR (400 MHz; DMSO-d_6): δ 8.49 (s, 1H), 7.32 (s, 1H), 6.32 (s, 2H), 2.48 (q, J = 7.5 Hz, 4H), 1.08 (t, J = 7.5 Hz, 6H); ^{13}H NMR (101 MHZ; DMSO-d_6): δ 150.2, 144.2, 131.93, 112.7, 23.0, 14.38; HRMS (EI, magnetic sector): calcd for $C_{10}H_{14}O_2$ 166.0993, found 166.1007.

*2,6-Diethyl-4-methoxyphenol (**16**)*. Methanol (15mL) and 2,6-diethylhydroquionone (0.95g; 5.7mmol) were placed in a 100mL round bottom flask equipped with a stir bar and reflux condenser. Carefully, 4.5mL of concentrated sulfuric acid was added and the reaction mixture was heated to reflux for ~4 hours. Once cooled the, the reaction mixture was poured into water followed by extraction with ether (three times). The combined organic extracts were dried with $MgSO_4$, filtered, and concentrated under reduced pressure. The product was isolated by column chromatography (10% EtOAc in hexanes). Two recrystallizations out of hexanes (minimum of hexanes at room temperature, followed by chilling on dry ice resulted in rapid crystallization) afforded the 2,6-diethyl-4-methoxyphenol as white needles (0.39g, 38%); mp 34-36°C; 1H NMR (400 MHz; DMSO-d6): δ 7.58 (s, 1H), 6.49 (s, 2H), 3.65 (s, 3H), 2.54 (q, J = 7.5 Hz, 4H), 1.10 (t, J = 7.5 Hz, 6H). 13C NMR (101 MHz; DMSO-d6): δ 152.5, 145.6, 132.0, 111.6, 55.1, 23.2, 14.4; HRMS (EI, magnetic sector): calcd for C11H16O2 180.1150, found 180.1140.

2,6-Diisopropylhydroquinone. The same general procedure for the preparation of 2,6-diethylhydroquinone was used in the preparation of 2,6-diisopropylhydroquinone from 2,6-diisopropylphenol (6.04g; 33.9mmol). The product was isolated by column chromatography (30% EtOAc in hexanes) and recrystallized out of hexanes affording 2,6-diisopropylhydroquinone as white leaflets (1.34g, 20.4%); mp 94-96°C; 1H NMR (400 MHz; DMSO-d6): δ 8.49 (s, 1H), 7.26 (s, 1H), 6.37 (s, 2H), 3.23 (sept., J = 6.9 Hz, 2H), 1.10 (d, J = 6.9 Hz, 12H); 13C NMR (101 MHz; DMSO-d6): δ 150.7, 142.75, 136.9, 109.4, 26.2, 23.0; HRMS (EI, magnetic sector): calcd for C12H18O2 194.1306, found 194.1297.

*2,6-Diisopropyl-4-methoxyphenol (**17**)*. Methanol (20mL) and 2,6-diisopropylhydroquionone (1.25g; 6.4mmol) were placed in a 100mL round bottom flask equipped with a stir bar and reflux condenser. Carefully, 6mL of concentrated sulfuric acid was added and the reaction mixture was heated to reflux for ~4 hours. Once cooled the, the reaction mixture was poured into water followed by extraction with ether (three times). The combined organic extracts were dried with $MgSO_4$, filtered, and concentrated under reduced pressure. The product was isolated by column chromatography (10% EtOAc in hexanes). After drying under vacuum, the residue was chilled (-20°C) affording 2,6-diisopropyl-4-methoxyphenol as a beige crystalline solid (1.06g, 79.5%); mp 48-50°C; 1H NMR (400 MHz; DMSO-d6): δ 7.53 (s, 1H), 6.51 (s, 2H), 3.66 (s, 3H), 3.28 (sept, J = 6.9 Hz, 2H), 1.13 (d, J = 6.9 Hz, 12H); 13C NMR (101 MHz; DMSO-d6): δ 153.0, 144.2, 136.9, 108.3, 55.0, 26.4, 22.9. HRMS (EI, magnetic sector): calcd for C13H20O2 208.1463, found 208.1487.

QUANTIFICATION AND STATISTICAL ANALYSIS

Unless otherwise indicated all experiments were carried out in three independent replicates and the mean ± SD are denoted in the appropriate figures and their corresponding captions.

DATA CODE AND AVAILABILITY

The datasets supporting the current study have not been deposited in a public repository because of the large size and the diversity of the results, but are freely available from the lead author on request.